UNIVERSITY OF CINCINNATI

MAY 16 , 20 01

I, Jill E. Krutz **,**

hereby submit this as part of the requirements for the degree of:

Masters of Science

in:

Mechanical Engineering

It is entitled:

Design of a hydraulic actuator test stand for non-linear analysis of hydraulic actuator systems.

Approved by:

Prof. David Thompson

Prof. Edward Berger

Prof. Randall Allemang

Design of hydraulic actuator test stand for non-linear analysis of hydraulic actuator systems.

A thesis submitted to the

Division of Research and Advanced Studies
of the University of Cincinnati

In partial fulfillment of the requirements
for the degree of

MASTER OF SCIENCE

In the Department of Mechanical, Industrial, and Nuclear Engineering
Of the College of Engineering

2001

By

Jill E. Krutz

B.S., Purdue University, 1998

Committee Chair:
Prof. David Thompson
Committee:
Randall Allemang
Ed Berger

Abstract

Stability is imperative in the design of hydraulic systems. Servo-hydraulic systems are inherently non-linear creating various nuances when analyzing the stability of the system. Friction, port flow, saturation, impact loading, line dynamics, and boundary conditions are a few of the many non-linearities found in servo-hydraulic systems which are to be analyzed using advanced non-linear stability analysis techniques. Some effects of instabilities induced by non-linearities such as pressure oscillations, noise, etc., can be detrimental to the stability or operation of hydraulic systems especially when the design is near the envelope of stability.

This thesis presents preliminary research on the various non-linearities found in hydraulic systems. A test stand has been developed to test the hydraulic cylinder system dynamics, with the inclusion of a mass-spring-damper system. An experimental modal analysis was performed on the hydraulic test stand to provide helpful information regarding the natural frequencies of the structure to insure that these frequencies do not lie near the natural frequencies of the hydraulic systems. Initial non-linear dynamic testing was completed on two hydraulic cylinders, consisting of finding the breakaway friction forces of the hydraulic cylinders.

Acknowledgements

Thank you to :

Prof. David Thompson
Prof. Randy Allemang
Prof. Ed Berger
Prof. Gary Krutz
Jeremy Korniak
Amit Shukla
Art Case
Jeff Hylok
Hal George
Parker Hannifin
Seven Letters
PCB Piezotronics

For all your help throughout my pursuit of my Master of Science in Mechanical Engineering, your help was essential.

Table of Contents

Table of Figures

Chapter 1: Introduction

The usage of fluid power can be traced back to the ancient Egyptians who used waterwheels as a prime mover. These first fluid power systems depended upon a high flow of fluid at low pressure. In the 1650's Pascal developed his laws on hydrostatics. It was not until 1795 that Joseph Bramah applied these laws and developed the first hydrostatic press, creating the first pressurized hydraulic machine and control system, and founding the fluid power industry, as we know it today.

Fluid power is defined as transmitting and controlling energy through the use of a pressurized fluid. Within fluid power there are two branches - hydraulics and pneumatics. Hydraulics use oils as the pressurized fluid, while pneumatics use air as the pressurized fluid. (Krutz, 1999) The focus of this research is only on hydraulic systems. Within hydraulic systems there are two main types of actuating devices - rotary and linear. A linear actuating system will be used in this research.

1.1 Applications of fluid power systems

Fluid power systems have a multitude of uses due to their ability to handle large force to weight ratios. Earth moving industries such as mining and construction use hydraulics to provide "muscle" and handle the overwhelming loads. Machines such as crushers, cranes, shovels, drills, hammers, classifiers, and rollers use hydraulics. Hydraulics also allow the driver to control implements from the cab for example, hydraulics are used to control the bucket on the

excavator in Figure 1.1. The fluid power systems are used heavily in the agricultural industry driving conveyors, harrows, harvesters, combines, and tractors. Fluid power systems also raise and lower implements such as plows for easy attachment and detachment, to the tractors and combines. Braking, power steering, power windows, landing gear control, as well as controlling ailerons, rudders elevators, and trim tabs are examples of hydraulic systems prevalent in mobile vehicles such as cars, trucks an/d airplanes. Hydraulics can also control movement for combat vehicles, submarines, shipping vessels, and missile artillery. Even the entertainment industry uses hydraulic motion control in roller coasters, special effects, animations, virtual reality situations, and simulators. (Pease, 1967 and Fitch & Hong, 2000)

Figure 1-1: Caterpillar Hydraulic Excavator using hydraulic controls to position a large section of piping. (Courtesy of www.cat.com)

1.2 Fundamental Design/Analysis Issues

The design of hydraulic systems can be quite overwhelming. There are entire books available on basic hydraulic design such as *Basic Fluid Power* by Pease (1967), and *Hydraulic Control Systems* by Merritt (1967). In addition to these textbooks, hydraulic manufacturers such as Parker Hannifin, Moog, and Eaton have their own design manuals. In the past few years, much of the design work

can be done using one of the many computer programs available to aid hydraulic system design. These programs have been developed using linearized modeling and “rules of thumb” developed through years of experience, and are quite adequate for the development of a standard highly stable hydraulic control system. These design practices tend to be experience-based, can often be empirical, and difficult to generalize to large-scale systems. Today, higher performance systems have a tendency to operate as close to the edge of the stability envelope as possible.

Stability is imperative in the design of hydraulic systems. Servo-hydraulic systems are inherently non-linear creating various nuances when analyzing the stability of the system. Friction, port flow, saturation, impact loading, line dynamics, and boundary conditions are a few of the many non-linearities found in servo-hydraulic systems which are to be analyzed using advanced non-linear stability analysis techniques. Some effects of instabilities induced by non-linearities such as pressure oscillations, noise, etc., can be detrimental to the stability or operation of hydraulic systems. This study should help us better understand analytically the non-linearities in hydraulic systems, using both computer-based computations as well as experiments verifying the computer findings. This methodology will facilitate a more comprehensive understanding of system-level interactions, allowing for operating conditions closer to the edge of the stability envelope.

To handle the more complex, large-scale, high performance systems, a more rigorous analysis-based procedure is needed. New analytical procedures are

now feasible due to the combination of three factors: (1.) large advances in computational capability in recent years; (2.) the application of more rigorous non-linear stability theory; and (3.) better empirical system understanding such as the work done by Fitch and Hong (2000) as well as Stecki (2000).

The numerical modeling using non-linear stability analysis will be verified using a basic hydraulic actuator test system. Section 4.2 details the design of this hydraulic system. A structure has been designed to support the hydraulic system as well as the physical loads applied against the cylinder. The design of this structure is detailed in Section 4.3.

The initial system testing of the stand will be comprised of vibrations testing, and characterization of the friction breakaway forces in the hydraulic actuator. The vibrations testing will involve finding the modes and mode shapes of both the base of the structure and the entire structure. The characterization of the friction forces will allow for a better understanding of this phenomenon and the sealing arrangement of the cylinder so it can be correctly introduced to the mathematical computations.

1.3 Thesis Outline

In this thesis, Chapter One introduces the concepts of hydraulic systems and stability. Chapter Two overviews previous analytical stability predictions for hydraulic systems, and includes the literature review. Chapter Three discusses the fundamentals of linear modeling and gives and introduction to some non-linear dynamics. Chapter Four describes the analysis and design of the

hydraulic test stand that will be used for non-linear dynamics testing. Chapter Five summarizes impact vibration testing and details the vibration testing done on the stand and the results of those tests. Chapter Six discusses some fundamentals of friction and tribology and details the testing methods used to determine the breakaway pressures in the hydraulic cylinders including the results from the testing. Finally, Chapter Seven overviews possible future research.

Chapter 2: Background

With so many different applications of fluid power as listed in Section 1.1, one would expect that fluid power systems must have significant advantages over other driving systems such as electromechanical systems. In addition to the large force to weight ratio characteristic, advantages in using fluid power systems are plentiful such as the fact that oil doubles as a lubricant, and removes heat easily; they have no phenomenon comparable to magnetic saturation in electrical machines leading to higher positional accuracy; they have high response speeds or higher loop gains and bandwidths are possible; large speed ranges are possible without damage; hydraulic actuators have high stiffness, allowing little drop in speed as loads are applied; and system control can be relatively easy relying on valves and pumps. There are also some disadvantages of using fluid power systems: hydraulic systems tend to leak oil; the components can be expensive due to the high machining tolerances required; each fluid is operational in certain temperature ranges, although, now there are many different types of fluids available; contamination of the oil can cause catastrophic failure of the system; they are more cumbersome than electrical systems for low power signals; design procedures for fluid power systems are complex and rely on vast knowledge of fluid flow; and their non-linearities can cause unforeseen oscillations of the systems when incorrectly designed. (Merritt, 1967)

2.1 Hydraulics

Basic fluid modeling can be found in texts such as Fox and McDonald (1992), Welty, *et al.* (1990) and Geankoplis (1993). These texts overview the orifice flow laws, continuity equations, Bernoulli's Law, the Navier-Stokes Equation, and pressure loss in lines due to friction. These concepts are integral to the hydraulic system design.

Fluid power has been extensively researched due to the vast array of applications possible. Pease (1967) and Henke (1983) are two of hundreds of references that give the basics of fluid power design. These references are great for learning some of the overall nuances found in fluid power design. The more conventional detailed modeling of hydraulic systems have been specified by Anderson (1988), Johnson (1995), Merritt (1967), McCloy and Martin (1973), Blackburn *et al.* (1960), and Fitch and Hong (2000). Anderson and Johnson focus on electrohydraulic systems specifically incorporating the electronic controls into the hydraulic system design. Merritt (1967) as well as McCloy and Martin (1973) assembled much of the empirical and practical information available on the design of hydraulic systems. Blackburn *et al.* (1960) included the non-linear dynamics of a hydraulic system with a single stage pressure relief valve. Fitch and Hong (2000) have taken the conventional information on hydraulic component design and selection and have incorporated computer-based design into the equation.

There are many papers related to specific hydraulic models. One such paper, by Margolis and Hennings (1994), found some fundamental parameter groupings that expose the instabilities in hydraulic systems that create the “singing” or “chirping” of a hydraulic servo valve. They used Laplace theory to model the two-stage hydraulic servo valve and used Taylor series expansion to linearize the model. Elleman and Piche (1994) examined the conventional turbulent orifice flow formula, which tends to cause numerical difficulties when using a numerical integrator and the pressure drop is near zero. They propose to replace the infinite derivative of the orifice flow formula with a finite derivative by creating a new two-regime formula for orifice flow, using empirical formulas.

Pump dynamics play a large role in stability of a hydraulic system. Pumps in general do not provide a smooth flow, but a pulsated flow. This can be minimized by the addition of an accumulator near the pump, but the pump flow dynamics need to be properly understood to specify the correct accumulator. Johnston and Longmore (1997) reviewed how to rate hydraulic pumps for noise potential. While looking at different possibilities they found that the internal ripple alone could only work well as a rating with low impedance circuits. Anechoic pressure and frequency are good ratings except they do not help determine the line size needed as a connection to the pump. They determined that the anechoic acoustic power is a good way to rate pumps. A weight system can be introduced before summing the individual powers from each harmonic.

2.2 Line Dynamics

The transmission line dynamics need to be taken into account when creating a non-linear model of a complete hydraulic control system. When the operating condition changes, a wave will travel along the pipe or hose lines. These waves can have a significant impact on the system if the frequency of the waves is close to the natural frequency of the system. There has been a plethora of research done regarding various aspects of transmission line dynamics. Basic acoustic resonant mode shapes found in pipes can be found in physics texts such as Serway (1992) or reference books such as Heald (1998). Taylor *et al* (1997) developed experimental validation techniques of transient friction flow models for both laminar and turbulent regimes. Longmore *et al* (1997) present methods that can obtain the dynamics of the hose walls during transient flows.

2.3 Friction Analysis

Friction is a complex phenomenon that is integral to life. It has positive effects when applied to power transmission devices such as clutches and brakes, but normally the goal is to reduce friction to reduce the energy exhausted by friction. Blau (1996) and Seirig (1998) have compiled information on friction theory. Blau (1996) focuses on friction theory itself, while Seirig (1998) focuses on the effects lubrication has on friction. Many hydraulic system design references, such as Johnson (1995), Viersma (1980), and Merritt (1967), include sections on friction within cylinders, valves and motors. Johnson (1995) gives a good explanation of the friction characteristics found in hydraulic systems. Viersma (1980) proves

that the Coulomb friction forces in hydraulic cylinders actually have no stabilizing effect, while Johnson (1995) claims that friction can be the only force that prevents sustained oscillations in feedback systems. Merritt (1967) relays the importance of the friction non-linearities including the relations between friction and backlash. Embedded in the friction theory is sealing technology. Seals are the contact surfaces that cause the friction. Muller (1998), Horve (1996), and Mayer (1973) detail seal design. Muller (1998), Horve (1996), and Mayer (1973) each devote a section to hydraulic sealing and Muller (1998) details the relation between friction and the seals.

2.4 Experimental Modal Analysis

Modal analysis is the study of the dynamic characteristics of a mechanical structure. This technique uses basics in structural dynamics to find the natural frequencies and their corresponding modes of a structure. To find the natural frequencies of an existing system, experimental data is taken to determine the frequency response function between the forces and responses and the modal parameters are estimated from models of frequency response functions. (Allemang, 1999)

In addition to troubleshooting vibration problems, experimental modal analysis can be used to correct or verify finite element analysis; develop mathematical models in sensitivity analysis, impedance modeling and modal modeling; and evaluate design changes to a structure. For most mechanical systems in operation, analytical information does not exist. The modal parameters

ascertained using experimental data offer a check and balance system to the corresponding information found analytically. (Allemang, 1999)

2.5 Non-linear Analysis of Hydraulic Systems

Research on the non-linear modeling of hydraulic actuator systems at the University of Cincinnati has been ongoing. G. Kremer (1998) developed a computer program that uses non-linear analysis to aid in the design of hydraulic control systems by finding the nearest distance and direction, in parameter space, to instability of an operating point. Kremer specifically used bifurcation theory as explained in Jordan (1999). A. Shukla (2000) is expanding this technique to fully integrate the generalized non-linear analysis into hydraulic control system design.

Chapter 3: Fundamentals of Linear System Modeling and Non-linear Dynamics

The design of systems is heavily dependent on system modeling because it greatly reduces the design time. The ability to correctly predict how a system design will run allows for fewer iterations of a design. Exact system modeling can be very complex and extensive due to the non-linear nature of the universe. Instead of using exact models in system design, linearized versions are often used. This still requires lengthy iterations of calculations and requires the inclusion of large factors of safety, but still tends to be faster than exact system modeling because the model is greatly simplified. With the advancement of technology, and the increased speed for calculations, the non-linear, more exact models can be used, allowing the designs to be closer to the edge of stability.

3.1 Linear modeling of hydraulic systems

For dynamic analysis, hydraulic systems are often modeled assuming the system is comprised of fluid volumes separated by sharp edged orifices, as seen in Figure 3-1. Such models are used in many industries, especially the automotive industry. This low order model, with enough detail, can correlate well with experimental data. Within this model, there are three types of equations used: equations of motion, continuity

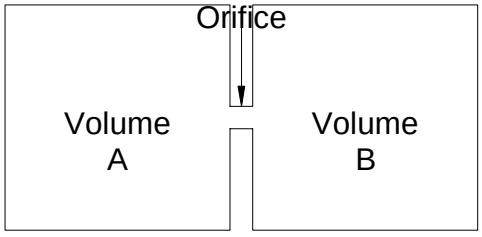

Figure 3-1: Simple fluid model of a hydraulic system using fluid volumes and a sharp edged orifice.

equations, and orifice equations. These equations are discussed further in the next three sections.

3.1.1 Equations of motion

The equations of motion define the movement of the mass elements such as the piston, the load, and the valve spool. These equations also take into account the physical damping and spring constant of the system as shown in Figure 3-2. Equation 3-1 is the generalized form of the equation of motion.

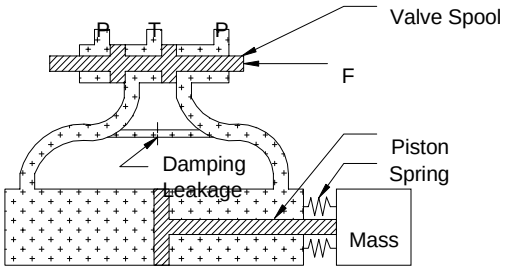

Figure 3-2: Mass Elements within a basic hydraulic system.

$$\Sigma F = m\ddot{x} \qquad \textbf{Eqn 3-1}$$

Where ΣF is the sum of external forces, m represents the mass element, and $\ddot{x}$ is the acceleration of the mass elements. Equation 3-1 can be expanded to include the damping and spring constant of the system as seen in Equation 3-2.

$$m\ddot{x} + b\dot{x} + kx = \Sigma F \qquad \textbf{Eqn 3-2}$$

Where $\dot{x}$ is the velocity of the mass element, x is the position of the mass element, b is the damping constant, and k is the spring constant.

3.1.2 Continuity equation

The continuity equation governs the conservation of mass in a fluid volume. The total flow into the system must equal the total flow out of the system plus the accumulation within the system as stated in Equation 3-3,fs

$$\Sigma Q_{in} = \Sigma Q_{out} + Q_{Accum} \qquad \textbf{Eqn 3-3}$$

where Q_{in}, Q_{out}, and Q_{Accum} represent the flow in and out of the system and the accumulation within the system respectively, as depicted in Figure 3-3. The accumulation within the system includes the flow consumed by expansion of the control volume, and the compressibility flow resulting from pressure changes, as stated in Equation 3-4,

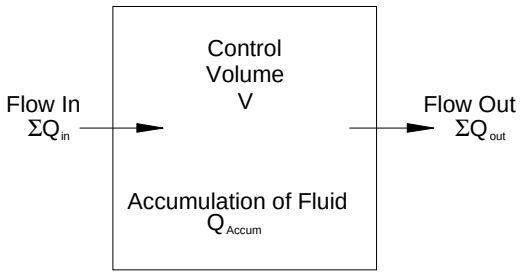

Figure 3-3: A fluid depiction of the conservation of mass theory.

$$Q_{Accum} = \frac{dV}{dt} + \frac{V}{\beta_{eff}} \frac{dP}{dt} \qquad \textbf{Eqn 3-4}$$

where V is the control volume (in^3), t is time (s), β_{eff} is the effective bulk modulus of the fluid, and P is the pressure within the fluid volume (psi). The effective bulk modulus is a function of the entrained air (*%air*), the bulk modulus of the fluid with no entrained air (β), and the pressure within the fluid volume (P_{vol}), as shown in Equation 3-5,

$$\beta_{eff} = \frac{1}{\frac{1}{\beta} + \frac{\%air}{1.4(P_{vol} + P_{atm})}} \qquad \textbf{Eqn 3-5}$$

where P_{atm} is the atmospheric pressure (psi). Most hydraulic oils can hold up to 10% entrained air, greatly varying the effective bulk modulus of the fluid. (Merritt, 1967)

3.1.3 Orifice equation

Orifice flow can be either laminar or turbulent, but most hydraulic systems are designed for turbulent flow. The orifice equation, as stated in Equation 3-6, defines the relationship between the pressure drop across the orifice (ΔP) to the flow through the orifice (q),

$$q = c_D A_{orifice} \sqrt{\frac{2}{\rho} |\Delta P|} \, \mathrm{sgn}(\Delta P) \qquad \textbf{Eqn 3-6}$$

where $A_{orifice}$ is the cross sectional area of the orifice (in^2), ρ is the density of the fluid (lb_m/in^3), c_D is the discharge coefficient, and the signum function, $sgn(\Delta P)$, returns the sign of the pressure drop. Figure 3-4 shows an orifice in a pipe section. The sign of the pressure differential determines the direction of flow; the fluid flows from the higher-pressure side of the orifice to the lower pressure side. The discharge coefficient is normally valued at 0.6 for sharp edged orifices when the Reynolds number is greater than 4000, or the system is within the turbulent flow regime. (Fitch & Hong, 2000)

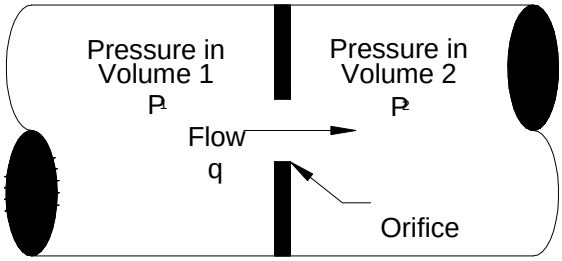

Figure 3-4: Flow through an orifice within a section of pipe.

For the development of the linear model, the orifice equation needs to be linearized, as shown in Figure 3-5, because the relationship between the flow and pressure is non-linear. This will be done using Taylor series expansion. Equation 3-7 shows the generalized form of Taylor expansion (Bay, 1999).

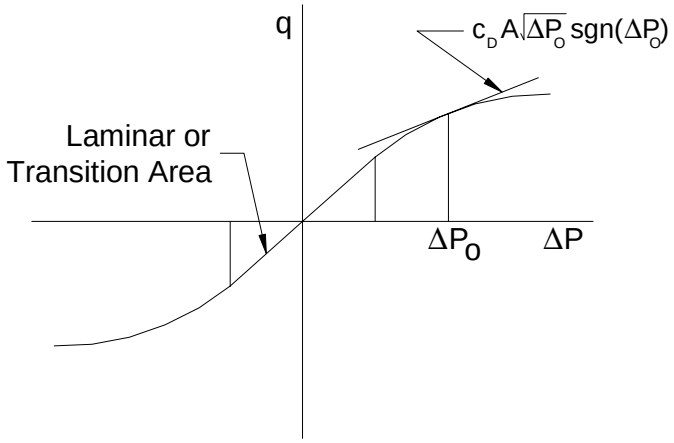

Figure 3-5: Linearizing a non-linear function.

$$f(x) = \sum_{1}^{\infty} \frac{1}{n!} \left. \frac{f(x)}{dx} \right|_{x=x_0} (x - x_0)^n \qquad \textbf{Eqn 3-7}$$

Only the zeroth and first order terms of the Taylor expansion are used in linearization of a non-linear equation. This transforms the orifice equation into Equation 3-8,

$$q = c(\Delta P) \qquad \textbf{Eqn 3-8}$$

where *c* is the constant of linearization and is defined in Equation 3-9,

$$c = \frac{c_D A_O}{\sqrt{\frac{2}{\rho}\Delta P_O^2}} \frac{2}{\rho} \qquad \textbf{Eqn 3-9}$$

ΔP_O is the initial operating point pressure difference across the orifice.

When using a linearized system it is assumed that the system perturbations stay within the local area of the initial operating point. Figure 3-6 depicts the non-linear function that represents the relationship between flow and pressure drop and is linearized equation near ΔP_0. Note that as ΔP gets farther and farther from ΔP_0, the linearized function becomes less and less accurate.

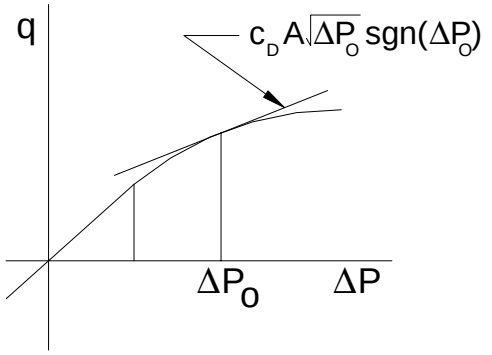

Figure 3-6: Linearizing a non-linear function.

3.2 Analyzing stability using a state-space technique

There are many ways to combine these equations to understand how the whole system will react under certain conditions. The two most popular ways are using transfer functions in conjunction with Laplace theory, and using state-space theory, as has been done throughout this research.

State-space theory uses a system of first-order differential equations that must be solved simultaneously, instead of a single, larger-order differential equation to describe the dynamics of a system. The order of the single differential equation defines how many equations will be in the set. For example, if the single differential equation is *n*-order, then *n* first-order equations will be needed. The variables used

to write these *n* first-order differential equations are called state variables (x_i), and can be chosen for convenience. The state is a collection of all the state variables, while the inputs (u_i) are a collection of all the inputs as shown in Equation 3-10.

$$\mathbf{x} = \begin{bmatrix} x_1 \\ x_2 \\ . \\ . \\ . \\ x_n \end{bmatrix}, \qquad \mathbf{u} = \begin{bmatrix} u_1 \\ u_2 \\ . \\ . \\ . \\ u_m \end{bmatrix} \qquad \textbf{Eqn 3-10}$$

The first-order differentials of the state variables are found as functions of the state variables and inputs and create the system of equations as defined in Equation 3-11.

$$\dot{\mathbf{x}} = \mathbf{f}\left(\mathbf{x}, \mathbf{u}\right) \qquad \textbf{Eqn 3-11}$$

The first-order differential equations can be put together in matrix form to create a linear state space model that can be expressed as Equation 3-12.

$$\dot{\mathbf{x}} = \mathbf{A}\mathbf{x} + \mathbf{B}\mathbf{u} \qquad \textbf{Eqn 3-12}$$

Where **A** and **B** are as follows:

$$\mathbf{A} = \left[\frac{\partial \mathbf{f}}{\partial \mathbf{x}}\right], \mathbf{B} = \left[\frac{\partial \mathbf{f}}{\partial \mathbf{u}}\right] \qquad \textbf{Eqn 3-13}$$

The states of a linear system at a given time can predict the state at all future times, assuming that all inputs and system dynamics are known. In addition, in this form, the states can easily determine many things such as the observability and controllability of variables as well as the stability of the system. (Bay, 1999)

The stability of the linear system is easily determined by finding the eigenvalues of **A**. The system is considered to be stable if the eigenvalues fall left of the imaginary axis. As the eigenvalues approach the imaginary axis, the system is considered to be less stable. As the eigenvalues get farther away from the imaginary axis toward the left, the system is considered to be more stiff. This is also true locally for the non-linear systems when Equation 3-14 is valid.

$$\mathbf{A} = \left[\frac{\partial \mathbf{f}}{\partial \mathbf{x}}\right]\Bigg|_{\mathbf{x}_0} \qquad \textbf{Eqn 3-14}$$

The crossover of this idea into to the non-linear system is very important to this research.

Chapter 4: Design of Hydraulic Actuator Test Stand

In order to verify the numerical modeling being completed by Shukla, experiments must reproduce similar results. To execute these needed experiments, a hydraulic actuator test stand is required. Test stand design involves taking many things into account in order to isolate a limited number of parameters of interest. First, the stand should be able to run at the operating points that are of interest. For this design, the system eigenvalues of interest from the standpoint of hydraulic control should ideally reside within the bandwidth of commercially available servo valves as well as be distinct from the structural eigenvalues of the stand. Moreover, the line dynamics eigenvalues should be identified so that the instabilities can be isolated. Therefore, a linearized numerical analysis will be done on the system first. Next, the stand must be structurally sound as well as easily modified, as this is the first iteration and changes to the stand may need to be performed. The stand should allow the loads placed on the hydraulic actuator to be varied. Finally, the stand needs to have the ability to be anchored to a large structure such as the floor or a seismic mass to reduce rigid body motion.

4.1. Linear State Space Model Parameter Analysis

Before beginning the design of the test stand, a linear, numerical model of the hydraulic system needs to be developed. This linear model confirms the results from Amit Shukla's non-linear model and also helps establish parameter ranges for the development of the test stand (Shukla, 2000).

The linearized program solves a system of six state-space equations for a hydraulic system consisting of a pump, a hydraulic actuator, two orifices and two accumulators as seen in Figure 4-1.

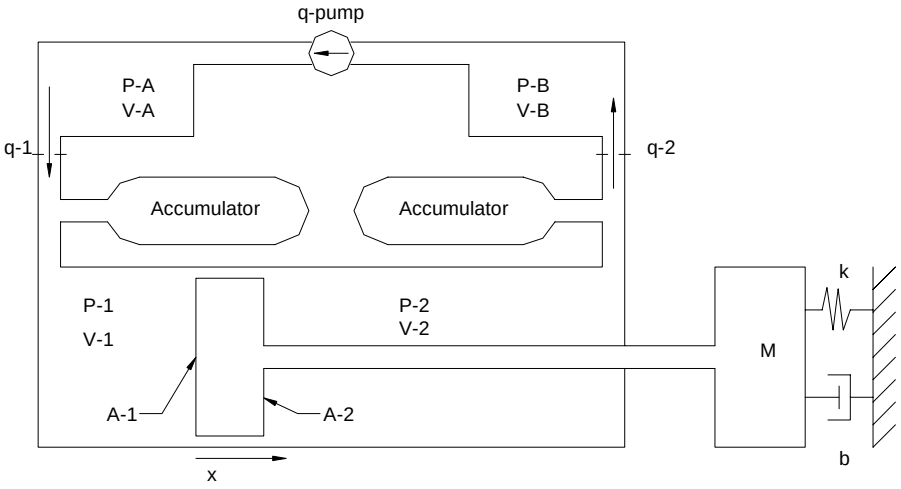

Figure 4-1. The hydraulic system numerically modeled by Eqn 4-1.

The states of the system are x_1 which is the pressure of the volume (V_A) between the pump and the first orifice (P_A), x_2 which is the pressure of the volume (V_1) between the first orifice and the piston (P_1), x_3 which is the pressure of the volume (V_2) between the piston and the second orifice (P_2), x_4 which is the pressure of the volume (V_B) between the second orifice and the pump (P_B), x_5 which is the position of the piston (x), and x_6 which is the velocity of the piston ($\dot{x}$). Equation 3-11 is the standard state space equation that relates these states,

$$\dot{\mathbf{x}} = \mathbf{A}\mathbf{x} + \mathbf{B}\mathbf{u} \qquad \textbf{Eqn 3-11}$$

where **x** represents the state vector and **u** represents the input vector. The system's sole input is the pump flow (q_{pump}). The derivative of each state is found beginning with the derivative of P_A by rearranging the continuity equation, as shown in the following equation.

$$\dot{P}_A = \frac{\beta_{eff}}{V_A}\left(q_{pump} - q_1\right) \qquad \textbf{Eqn 4-1}$$

Where β_{eff} is the effective bulk modulus, q_1 is the flow through the first orifice as seen in Figure 4-1. The derivatives of P_B, P_1, and P_2 can be found in a similar manner resulting in the next three equations,

$$\dot{P}_B = \frac{\beta_{eff}}{V_B}\left(q_2 - q_{pump}\right) \qquad \textbf{Eqn 4-2}$$

$$\dot{P}_1 = \frac{\beta_{eff}}{V_1}\left(q_1 - A_1\dot{x}\right) \qquad \textbf{Eqn 4-3}$$

$$\dot{P}_2 = \frac{\beta_{eff}}{V_2}\left(A_2\dot{x} - q_2\right) \qquad \textbf{Eqn 4-4}$$

where q_2 is the flow through the second orifice as seen in Figure 4-1, A_1 is the area of the piston face, A_2 is the annular area of the rod side of the piston (in), and $\dot{x}$ is the velocity of the piston (in/sec). These pressure derivatives are currently in terms of flow, and need to be transformed into terms of the states. The linearized orifice flow equation, Equation 4-6, represents the flows in terms of pressures, and will be used for the transformation,

$$q = c(\Delta P) \qquad \textbf{Eqn 4-5}$$

where c is the constant of linearization. The constants of linearization for each of the two orifices in the system are as follows,

$$c_1 = \frac{c_D A_{O1}}{\sqrt{\frac{2}{\rho}\Delta P_{O1}^2}}\frac{2}{\rho} \qquad \textbf{Eqn 4-6}$$

$$c_2 = \frac{c_D A_{O2}}{\sqrt{\frac{2}{\rho}\Delta P_{O2}^2}} \frac{2}{\rho}$$ **Eqn 4-7**

For the above equations, A_{O1} and A_{O2} are the cross sectional areas (in^2) of orifice one and orifice two respectively. The initial pressure differentials across the orifices are represented as ΔP_{O1} for $P_{01} - P_{0A}$ (psi), and ΔP_{O2} for $P_{0B} - P_{02}$ (psi).

The linearization of the flow equation assumes that the system flow and pressure drop is perturbed minimally near the nominal, or starting, operating point. The accuracy of the model is reduced as perturbations become large.

$$\dot{x}_5 = x_6$$ **Eqn 4-8**

The definition of velocity provides that the derivative of the piston position $(\dot{x}_5)$ is the velocity of the piston x_6, as stated in Equation 4-9. The derivative of the velocity of the piston is the acceleration of the piston and can be found using the system's equation of motion as shown below in Equation 4-10,

$$\ddot{x} = -\frac{b}{m}\dot{x} - \frac{k}{m}x - \frac{A_2}{m}P_2 + \frac{A_1}{m}P_1$$ **Eqn 4-9**

where b is the damping coefficient of the damping system (lb_m/s), k is the spring coefficient of the spring system (lb_m/s^2), and m is the mass load applied to the hydraulic cylinder (lb_m).

After finding all the derivatives of the states with respect to the states and inputs, the resulting system of equations can be arranged as follows.

$$\begin{Bmatrix} \dot{P}_1 \\ \dot{P}_2 \\ \dot{P}_A \\ \dot{P}_B \\ \dot{x} \\ \ddot{x} \end{Bmatrix} = \begin{bmatrix} \frac{-\beta_{eff} c_1}{V_1} & 0 & \frac{\beta_{eff} c_1}{V_1} & 0 & 0 & \frac{-\beta_{eff} A_1}{V_1} \\ 0 & \frac{-\beta_{eff} c_2}{V_2} & 0 & \frac{-\beta_{eff} c_2}{V_2} & 0 & \frac{-\beta_{eff} A_2}{V_2} \\ \frac{-\beta_{eff} c_1}{V_A} & 0 & \frac{-\beta_{eff} c_1}{V_A} & 0 & 0 & 0 \\ 0 & \frac{-\beta_{eff} c_2}{V_B} & 0 & \frac{-\beta_{eff} c_2}{V_B} & 0 & 0 \\ 0 & 0 & 0 & 0 & 0 & 1 \\ \frac{A_1}{m} & -\frac{A_2}{m} & 0 & 0 & -\frac{k}{m} & -\frac{b}{m} \end{bmatrix} \begin{Bmatrix} P_1 \\ P_2 \\ P_A \\ P_B \\ x \\ \dot{x} \end{Bmatrix} + \begin{bmatrix} 0 \\ 0 \\ \frac{\beta_{eff}}{V_A} \\ \frac{-\beta_{eff}}{V_B} \\ 0 \\ 0 \end{bmatrix} \{q_{pump}\} \quad \textbf{Eqn 4-10}$$

The eigenvalues of the matrix **A**, the 6 x 6 matrix found in Equation 4-10, then were graphed as parameters were perturbed from an initial operating point. Table 4-1 overviews the parameter variations and initial operating point for the perturbations.

Table 4-1: Initial values and perturbation ranges of parameters for the parameter study using the linearized numerical model.

Symbol	Parameter	Parameter Values				Step Size
		Initial	Min	Max	Units	
M	Mass	200	20	400	lb_m	10
D	Piston Diameter	3	1.5	3	in	0.1
L	Stroke/Cylinder Length	8	6	12	in	0.5
%air_ac	System Air Percentage	.20	0.02	0.4	%	0.01
q_{pump}	Pump Flow	25	0.5	50	in^3/s	0.5
d_r	Orifice Diameter	0.1	0.1	0.75	in	0.05
xref	Piston Starting Position	3	1	7	in	0.5
k	Spring Rate	1000	0	2000	lb_f/in	100
	Leak Damping		P1	P2		
X_dotref	Piston Velocity	1			in/s	
L1	Hose length in Va	36			in	
L2	Hose length in V1	6			in	
L3	Hose length in V2	6			in	
L4	Hose length in Vb	36			in	
dia	Shaft Diameter	1			in	
b	Damping Constant	4			$lb_f/(in/s)$	
rho	Density of oil	$.78 \times 10^{-4}$			$lb\text{-}sec^2/in^4$	
C_D	Flow Constant of Oil	0.6				
P_{atm}	Atmospheric Pressure	14			Psi	
Beta	Bulk Modulus	22,000				

The parameters are perturbed individually to see the effect each parameter variation has on the system. The individual perturbation of the mass, piston diameter, stroke length, system air percentage, pump flow, orifice diameter, piston starting position, and spring rate variables is discussed through the remainder of this section. The results of this parameter perturbation analysis are reflected in Figure 4-2 through Figure 4-9.

Figure 4-2 depicts the eigenvalues of [A] when the system is at its nominal or initial operating condition, per Table 4-1. One of the key design goals of the stand is to allow the eigenvalues of interest to reside within the anticipated bandwidth of the

servo valve as well as distinct from the structural natural frequencies of the stand and the line dynamics.

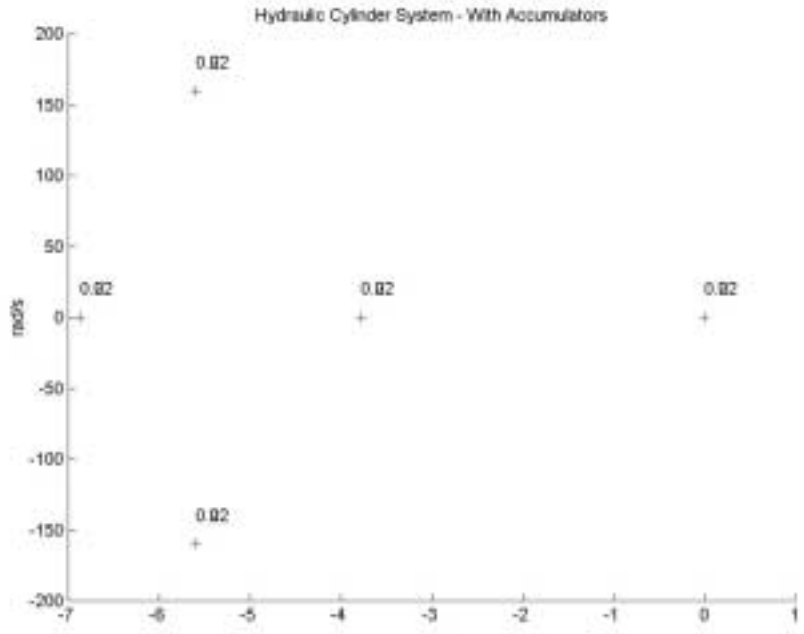

Figure 4-2: The eigenvalues of the initial operating condition.

When varying the air content in the system, the bulk modulus changes. The bulk modulus decreases, or the system becomes less stiff, as the air percentage increases. The bulk modulus equation (Merritt, 1967) is shown below:

$$\frac{1}{\beta_{eff}} = \frac{1}{\beta_{nom}} + \frac{\%air}{1.4(P_{atm} + P)} \qquad \textbf{Eqn 4-11}$$

The bulk modulus of oil assuming no air entrainment is represented by β_{nom}, P_{atm} represents the atmospheric pressure, P is the pressure of the oil, and *%air* is the percentage of air entrained in the oil. When using an accumulator that is loaded by pressurized air, the volume of air within the accumulator can be added to the entrained air, because the air has a much larger tendency to compress and so all

the air within the system will compress first whether it is entrained or a large pocket of air such as found in the accumulators.

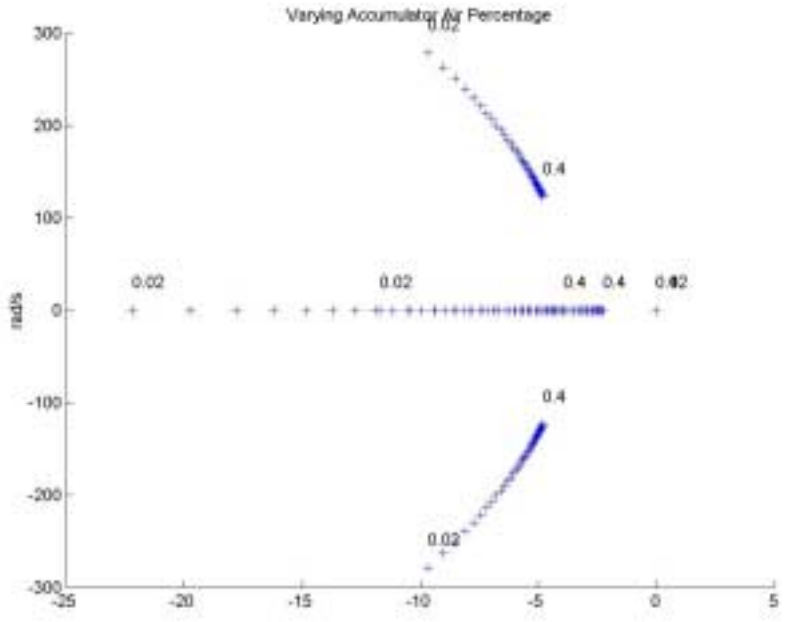

Figure 4-3: The eigenvalues when the system air percentage is perturbed from 2% to 40% air.

The eigenvalues in Figure 4-3 furthermore demonstrate that the system becomes less stiff, or closer to instability, as the air percentage increases. In addition, the system's natural frequencies also decrease as the air percentage increases. Changing the preload on the accumulators within the system will vary the volume of air within the accumulator, which in turn varies the system's air percentage.

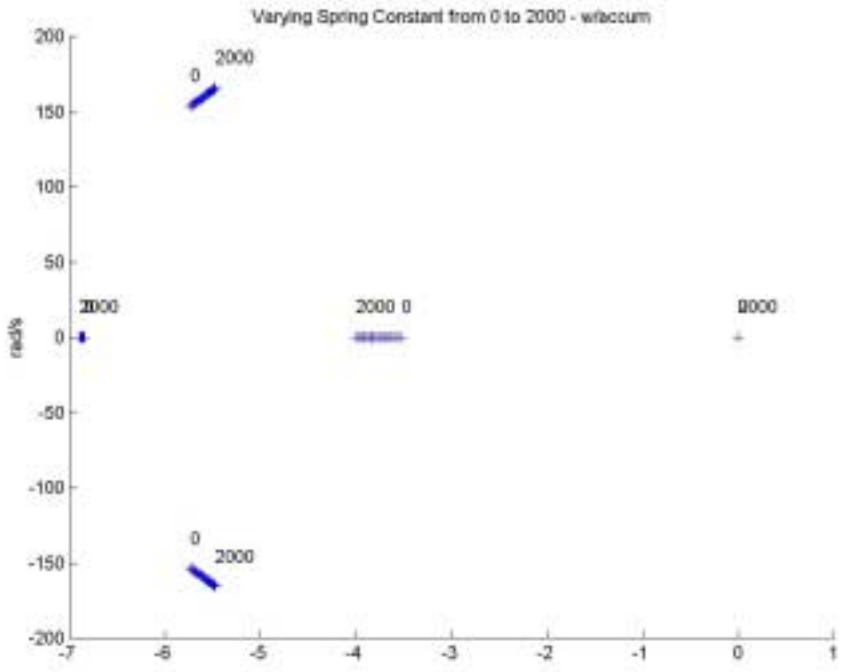

Figure 4-4: The eigenvalues when the spring constant *k* is varied from 0 to 2000.

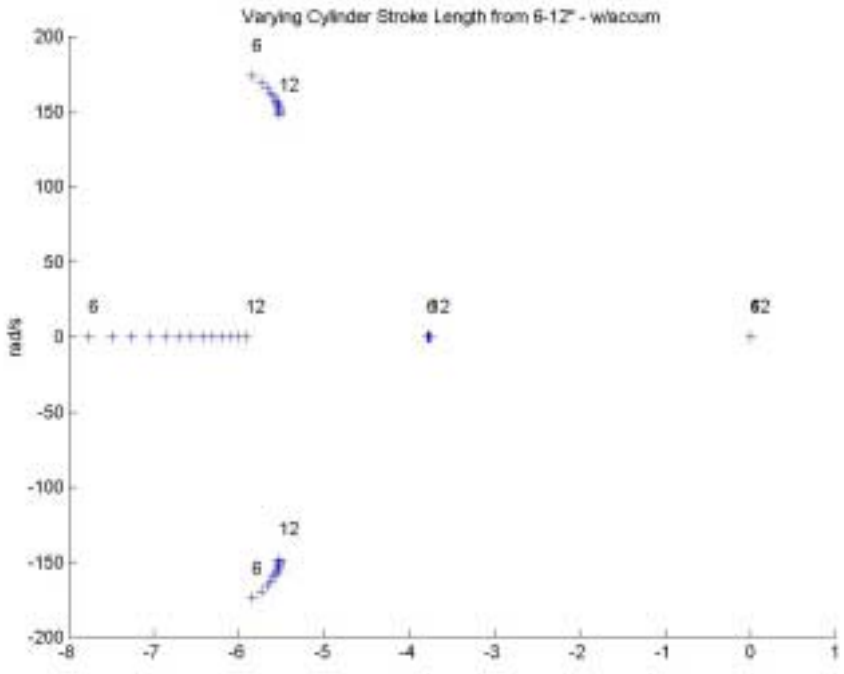

Figure 4-5: The eigenvalues when the cylinder stroke length is varied from 6" to 12".

When the spring constant is varied, as shown in Figure 4-4, there is minimal change in the stability or the natural frequency. The change that occurs shows that the system does become less stable and the natural frequency increases as the spring constant (*k*) increases. Therefore, the spring constant can be reasonable, and a small spring can be designed for the hydraulic test stand.

The cylinder stroke length variation seems to also have little effect on the system's stability and natural frequency, as shown in Figure 4-5. The system becomes slightly less stable and the natural frequency reduces slightly as the stroke length increases. This is not surprising since the majority of the oil volume in the system is found in the accumulators and the lines. This will allow the stroke length to be dictated by the physical testing requirements.

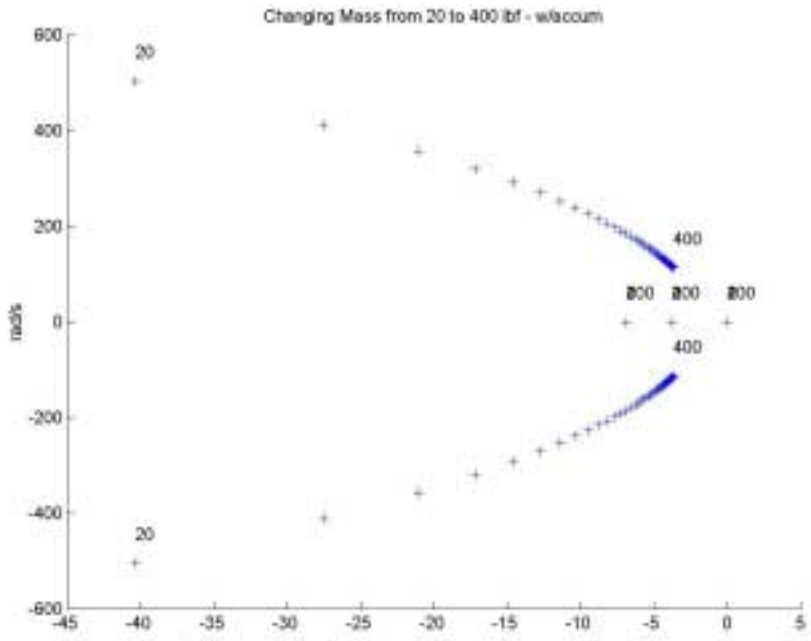

Figure 4-6: The eigenvalues when the mass *m* is varied from 20 lb_f to 400 lb_f in 10lb_f increments.

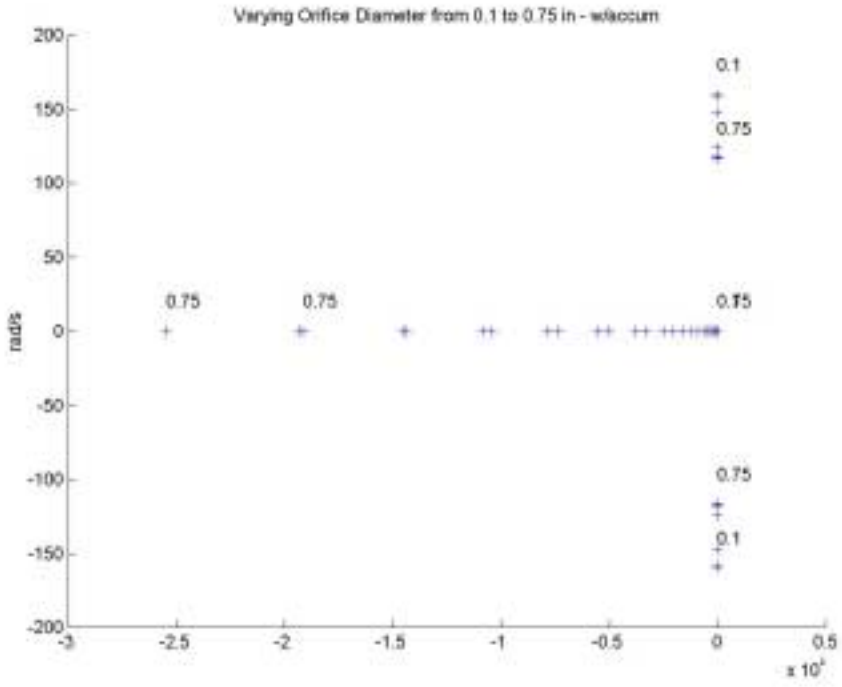

Figure 4-7: The eigenvalues when the orifice diameter is varied from 0.1-in. to 0.75-in.

Mass variation has a great effect on the system as shown in Figure 4-6. The stability and natural frequency decrease as the mass is increased. It is duly noted that the variations seem to vary exponentially, allowing the greatest change to the system to occur between 20 lb_f and 100 lb_f. This will allow the system to have a relatively small mass load, increasing the safety aspects of the design.

The orifice diameter change shows a large increase in the stability of the eigenvalues on the real axis, a minute decrease in the stability of the eigenvalues not on the real axis, and a small decrease in the natural frequency of the system as the orifice diameter is increased. As the orifice diameter becomes closer to the line diameter (or increases), the orifice should act like the pipe flow and less like an orifice.

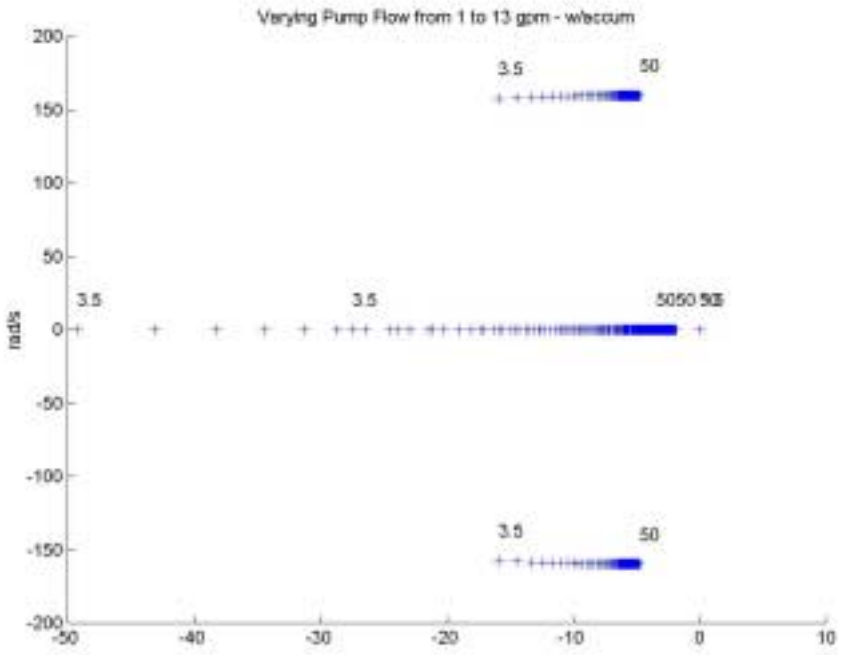

Figure 4-8: The eigenvalues when the pump flow q_{pump} is varied from 1 GPM (3.5 in^3/s) to 13 GPM (50 in^3/s).

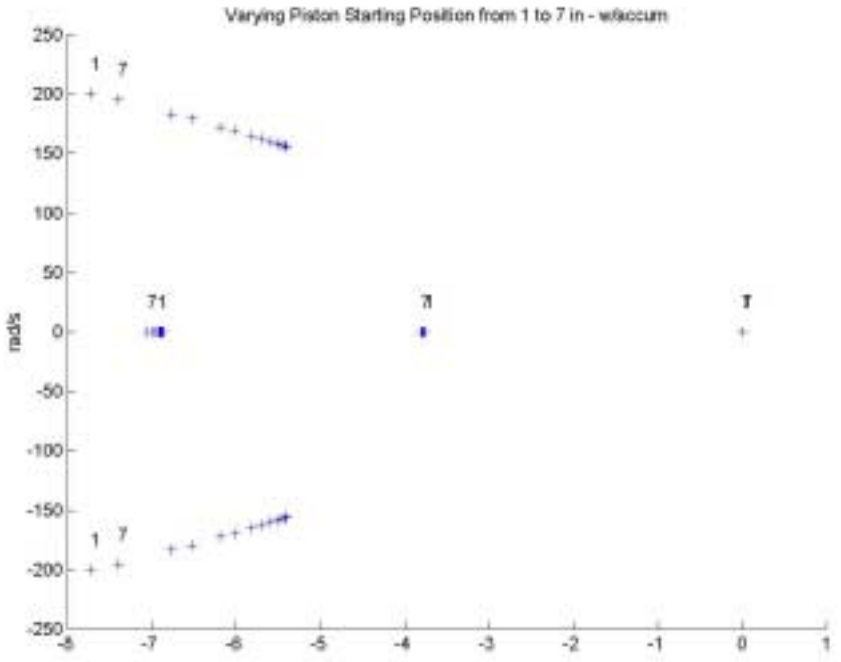

Figure 4-9: The eigenvalues when the piston initial position *x* is varied from 1 to 7 inches.

An increase of the initial pump flow has negligible effect to the natural frequency, but does decrease the stability of the system, as shown in Figure 4-8. For this perturbation, the flow constants c_1 and c_2 were altered to change with respect to the constant pump flow versus the initial pressure drop across the orifices, as shown in the following equations.

$$\Delta P_o = \frac{\rho}{2}\left(\frac{q_{pump}}{c_D A}\right)^2 \qquad \textbf{Eqn 4-12}$$

$$c_1 = c_2 = \frac{c_D^2 A_{orifice}{}^2 \frac{2}{\rho}}{q_{pump}} \qquad \textbf{Eqn 4-13}$$

Varying the initial position of the cylinder piston does change the stability of the system, but does little with the natural frequency. Figure 4-9 shows that the system is least stable when the initial position is in the middle, and the volumes are equal on each side of the cylinder, while the system is most stable when the initial position is at either end of the cylinder and the volumes on each side of the cylinder are the least equal. When designing the dynamic tests, this finding should be taken into account.

4.2. Design of Hydraulic System for the Hydraulic Test Stand

After evaluating how the parameters interact with each other in view of the testing objectives discussed previously, the nominal parameters of the hydraulic system were developed. Table 4-2 presents the parameter values for the hydraulic test stand.

Table 4-2: Hydraulic system parameters – nominal design values.

Parameter	Value
Maximum Piston Diameter	3 ¼”
System % air	20%
Maximum Mass	300 lb_f
Stroke/Cylinder Length	7”
Pump Flow	2 GPM
Orifice Diameter	0” – 3/8”
Piston Starting Position	3.5”
Spring Rate	Variable
Leak Damping	Variable

Figure 4-1 illustrates a simplified hydraulic system. In reality, this idealized hydraulic model is overly simplified; therefore a realistic, more detailed hydraulic system must be developed that mimics the actual system used for experimental testing. This system will include the pump, actuator, accumulators, and needle valves for the orifices as well as pressure transducers, control valves, and a filtration operation. The mass and spring are not considered part of the hydraulic system, but will be part of the test stand, while the damping effect will be implemented by inducing leakage using a needle valve. Figure 4-10 depicts the actual hydraulic system designed for the hydraulic test stand.

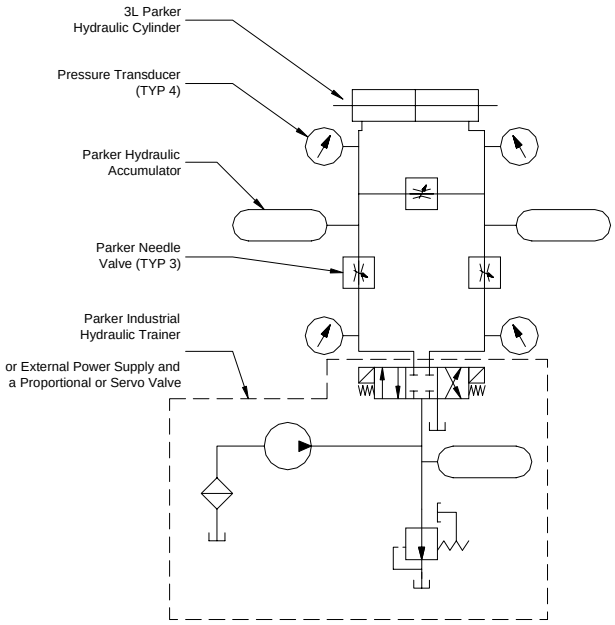

Figure 4-10: Hydraulic system for the hydraulic test stand.

The hydraulic system is composed of a power unit, a proportional valve, an actuator, three accumulators, three needle valves, four pressure transducers, and miscellaneous tubing and hosing. Some of these components are readily available in the laboratory, and are incorporated into the design while the other components are new.

The components within the dotted line in Figure 4-10 will initially be found on the Parker Industrial Hydraulic Trainer Bench. (Parker, 1999) These include the power unit (pump, motor, filtration, reservoir, relief valve, and needed tubing and fittings), the accumulator to compensate for the pump flow pulsations, and the proportional valve. Eventually, an external power supply and control valve system will be used in lieu of the Parker Trainer. The connections between the power unit and the proportional valve and the proportional valve and the rest of the system are composed of 3/8” hosing with quick disconnecting fittings. In the future, a servo valve will be mounted directly on the cylinder.

When sizing and placing an accumulator to compensate for pump pulsations, there are some key points to keep in mind. Viersma (1980) indicates that the accumulator needs to be placed within 30 cm (~1 ft.) of the pump and that the connection line between the accumulator and the main line be less than 5 cm (2 in) in length and have a volume smaller than 0.5-1 dm^3 (30-60 in^3) to influence the system accurately. The accumulator must also be preloaded correctly. The correct preload can be found using the charts in the Parker Hannifin accumulator selection brochures. (Parker, 1999) They correlate the preload to the operational pressure.

Accumulators can affect the system as if there is a larger volume of air entrained in the system, lowering the bulk modulus as well as the natural frequencies of the modes of the system. The pressure transducers will provide the pressures of each volume. The needle valves will be used as orifices to simulate large transmission line restrictions. Two valves separate the four basic volumes, the third allows for leakage between each side of the cylinder for damping purposes. The rest of the system is the basic hydraulic actuator system under study. In addition to the hydraulic system, a spring and mass system will be attached to the actuator completing the mass-spring-damper system.

Table 4-3 overviews the vendors and model numbers of the various components within the hydraulic system. Both existing and new components are listed.

Table 4-3: Components of the hydraulic system

Component	Model Number	Vendor	New/ Exist
Pump	On Trainer	Parker	Exist
Motor	On Trainer	Parker	Exist
Proportional Valve	On Trainer	Parker	Exist
Reservoir	On Trainer	Parker	Exist
Relief Valve	On Trainer	Parker	Exist
Filtration	On Trainer	Parker	Exist
Tubing	3/8” NPT fittings	Parker	Exist
Hosing	3/8” no-skive 301-6	Parker	Exist
Fittings (existing)	NS-371,372 –6FP	Parker	Exist
Needle Valve	On Trainer	Parker	Exist
Pressure Gauges	On Trainer	Parker	Exist
Accumulator	On Trainer	Parker	Exist
Actuator #1	2 ½ TC-3LXLTS34AX7.00 – NNC2N	Parker	New
Actuator #2	3 ¼ TC-3LXLTS34AX7.00 – NNC2N		New
Fittings (new)	NS-371,372 –6FP	Parker	New
Hosing (new)	3/8” no-skive 301-6	Parker	New
Pressure Transducer	PCB 1502A02FJ 1KPSIS	PCB Piezotronics	New
Tubing (new)	3/8” NPT fittings	Parker	New

4.3. Design of Structure

There are infinite ways to mount a hydraulic cylinder. Mounting the cylinder in the vertical direction holding up the load has been chosen to eliminate a friction load produced by the contact of the masses and a support. The vertical mount also allows the load to be aligned along the axis of the cylinder much more easily, reducing the possibility of an eccentric loading resulting in a moment and/or side load on the cylinder rod. With this decision, a feasible mount structure must be designed.

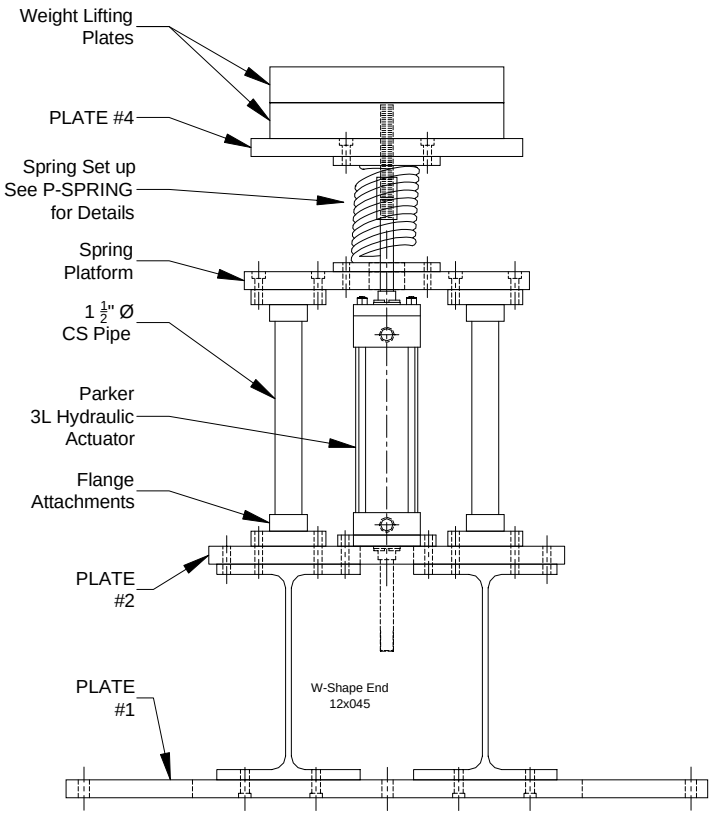

Figure 4-11: A side view of the hydraulic actuator test stand.

The design of the structure has to satisfy many requirements. The important requirements defined by the testing planned for this stand included: the ability to support the hydraulic system and masses; the ability to support to reaction forces from the hydraulic system; clearance for a double rod cylinder or the linear displacement transducer (LDT) of a single rod cylinder; highly stiff structure with the first flexible modes occurring away from the natural frequency of the hydraulic system; a support for the spring system as well as the mass system; the ability to be attached to the floor or seismic mass easily; safety of things near the test stand; and the ability to easily alter the machine.

The base plate or Plate #1 was designed to be a large enough footprint so that the machine would not be top heavy with the addition of mass up to 300 pounds to the

top of the machine. Plate #1 also includes a 4” on center bolt pattern with 5/8” boltholes so that the machine can be easily attached to the seismic masses on a plate similar to the ones already embedded in the seismic mass at the University of Cincinnati, Structural Dynamics Research Laboratory (SDRL).

The I-beams and Plate #2 were designed to be a very stiff structure. The I-beams were chosen because they are strong in the vertical direction, they are readily available, they would provide clearance for the LDT or a double-rod cylinder, and the plates can be easily attached to the flanges of the beams. The bolt pattern on the base of the I-beams is a 4” on center with 5/8” bolt-holes, so that Plate #1 can be removed and the test stand can still be attached to the seismic mass. To obtain a thickness for Plate #2, a simple deflection calculation was conducted for the plates with varying thickness and the flange. A design constraint set by Professor Thompson is the maximum static force on the plate at 12,000 lb_f, with the force being distributed over the area of the hydraulic mounting. The plate was assumed to be a plate simply supported at two ends with a distributed force in the center as shown in Figure 4-12 (a). The flange was assumed to be a cantilevered plate with a distributed force at the free end as shown in Figure 4-12 (b).

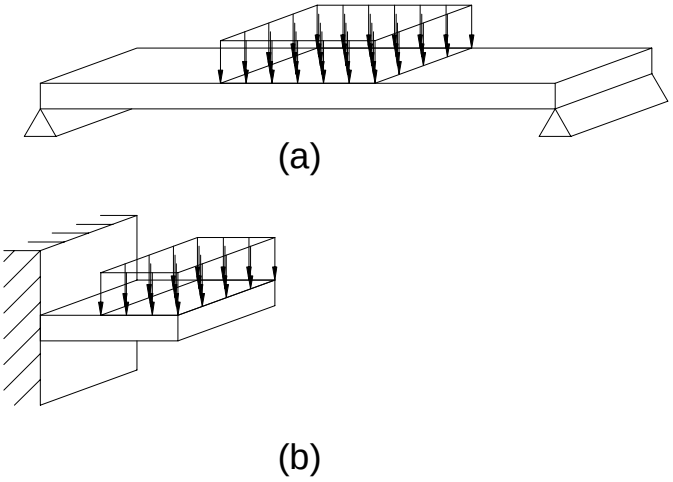

(a)

(b)

Figure 4-12: (a) The beam model used for Plate #2. (b) The beam model used for the flange of the I-beam.

The deflection equations used for the plate and the flange are Equation 4-14 and Equation 4-15 respectively,

$$\delta = \frac{-PL^3}{48EI} \qquad \textbf{Eqn 4-14}$$

$$\delta = \frac{-PL^3}{3EI} \text{ or } \delta = \frac{-PL}{EA} \qquad \textbf{Eqn 4-15}$$

The larger of the two

where δ is the deflection, P is the load, L is the length of the plate or flange, E is Young's Modulus (30 x 10^6 psi), A is the cross sectional area of the flange, and I is the inertial force. For multiple layers of materials, the inverse of the total deflection is the sum of the inverses of the deflection of each layer as shown in Equation 4-16.

$$\frac{1}{\delta_T} = \sum_i^n \frac{1}{\delta_i} \qquad \textbf{Eqn 4-16}$$

It was found that the deflection of the center of the plate, with the maximum load, should be 0.005 inches for a 1-inch plate and 0.01 inches for a ¾-inch plate, so a 1-inch plate was chosen. The thickness of the other large plates became 1-inch due to economical reasons.

The spring platform, or Plate #3, is designed to be removable, with the possibility of changing its height by replacing the pipes with different length pipes. A rod extension is added to the rod of the hydraulic actuator to support the mass system. The bolts were designed to be able to handle a quarter of the total load each. This resulted in 3/8” Grade 8 bolts with a 23 lb-ft. preload torque.

Design of Spring/Mass System

Hydraulic actuator systems are used to move and position large loads. In the test stand, the loads are represented by the spring and mass system. A spring is placed inline with the cylinder rod as shown below in Figure 4-13.

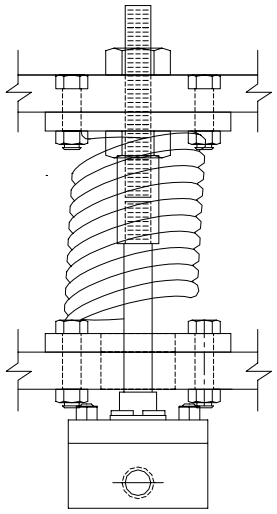

Figure 4-13: Spring set up on the hydraulic actuator test stand.

The spring will be attached at both ends to plates that attach to the structure. This will allow the spring to react in both compression and tension when necessary. The threaded rod will allow enough room in the spring set-up so that the spring coils will never touch each other.

Weight lifting weights will be used as the masses, allowing a large variation of mass to be included in the system, as well as they are more economically feasible than fabricating mass plates out of steel.

Design of Damping System (leakage)

Leakage damping is commonly used in electrohydraulic systems to increase stability across the cylinder. In future experiments, such as the parameter perturbation to find the stability envelopes, leakage will be used for damping purposes.

The set-up for leakage damping is a needle valve in parallel with the cylinder as shown in Figure 4-10. The needle valve will set the amount of damping required by the experiment by varying the orifice.

Chapter 5: Vibration Testing of the Hydraulic Actuator Test Stand Base

In the non-linear testing of the hydraulic systems, it is necessary that the structural natural frequencies are not near the natural frequencies of the hydraulic system. If this occurs, the vibrations within the system may resonate, increasing the amplitude and possibly causing catastrophic failure of the system or the structure. It is also important to have an idea of what the mode shape is at these natural frequencies. The mode shapes show the locations of largest motion where this catastrophic failure is most likely to occur, allowing for design changes if needed. The structural natural frequencies can be found by conducting an experimental modal analysis on the hydraulic test stand itself.

5.1 Fundamentals of Experimental Modal Analysis for Vibration Analysis

The natural frequencies and mode shapes of a mechanical system are parameters within vibration analysis. Vibration analysis is a study of the oscillatory motions and associated forces of a body. Vibration only requires a body to have mass and elasticity, therefore most mechanical structures experience vibration to some degree. (Thomson, 1993) The vibratory motion is a function of the system characteristics, and a function of the system excitation. System characteristics are often described as frequency response functions shown in Equation 5-1,

$$\begin{bmatrix} X_1 \\ X_2 \\ . \\ . \\ . \\ X_p \end{bmatrix} = \begin{bmatrix} H_{11} & H_{12} & . & . & . & H_{1q} \\ H_{21} & H_{22} & & & & . \\ . & & & & & . \\ . & & & & & . \\ . & & & & & . \\ H_{1p} & . & . & . & . & H_{pq} \end{bmatrix} \begin{bmatrix} F_1 \\ F_2 \\ . \\ . \\ . \\ F_q \end{bmatrix} \qquad \textbf{Eqn 5-1}$$

where ***X*** is the response vector, ***H*** is the frequency response function, or transfer function matrix, and ***F*** is the external force vector.

Within vibration analysis there is modal analysis theory. This is the concept that natural frequencies, damping factors and mode shapes for linear systems can be used to create a system model. The modal parameters create an optimal model or basis that can express the dynamics of a mechanical structure in response to varying initial conditions, and forcing functions. Using modal analysis based upon experimental data to find the modal parameters is labeled experimental modal analysis.

In experimental modal analysis, a few assumptions must be made at first. The system to be analyzed is assumed to be linear, and for a wide range of structures this is a valid assumption. The system is assumed to be time invariant; or the mass, stiffness, and damping of the system are constant and depend on factors that are not included in the model. It is assumed that the system obeys Maxwell's reciprocity law, or a force applied at degree-of-freedom *p* produces a response at degree-of-freedom *q* that is equivalent to the response at degree-of-freedom *p* when the same force is applied to degree-of-freedom *q* ($H_{pq} = H_{qp}$). The final assumption is that the system is observable, in other words, the input-

output measurements of the system contain enough information that a realistic behavioral model can be extracted from them. (Allemang, 1999)

Once these assumptions are made and verified, the first step, modal data acquisition, can occur. There are many different models and experiments that can be done that will produce effective data. The sinusoidal input-output model, the frequency response function model, the damped complex exponential response model and the general input-output model are four of the most commonly used models for experimental modal analysis. The last two models are composite approaches that involve intricate parameter estimation algorithms that are based on structural models. The sinusoidal input-output model is based on exciting the system in only frequency. The frequency response method originated out of the sinusoidal input-output model, but with the advent of the computer, it became a separate technique. In this method, the frequency response functions are measured by exciting a single or multiple points using the simple relationship found in Equation 5-1. (Allemang, 1999)

$$\begin{bmatrix} X_1 \\ X_2 \\ . \\ . \\ . \\ X_p \end{bmatrix} = \begin{bmatrix} H_{11} & H_{12} & . & . & . & H_{1q} \\ H_{21} & H_{22} & & & & . \\ . & & & & & . \\ . & & & & & . \\ . & & & & & . \\ H_{1p} & . & . & . & . & H_{pq} \end{bmatrix} \begin{bmatrix} F_1 \\ F_2 \\ . \\ . \\ . \\ F_q \end{bmatrix} \qquad \text{Eqn 5-1}$$

There are two types of excitation used in the frequency response function models: shaker excitation and impact excitation. Shaker excitation involves exciting the structure at a small number of points and collecting data at a large

number of points. A shaker is normally used as the excitation device. For impact excitation a specially designed hammer is used to excite the structure at a large number of points, while data is taken at a small number of points. In this research, impact excitation will be used. Figure 5-1 depicts a normal experimental set up for impact testing. (Allemang, 1999)

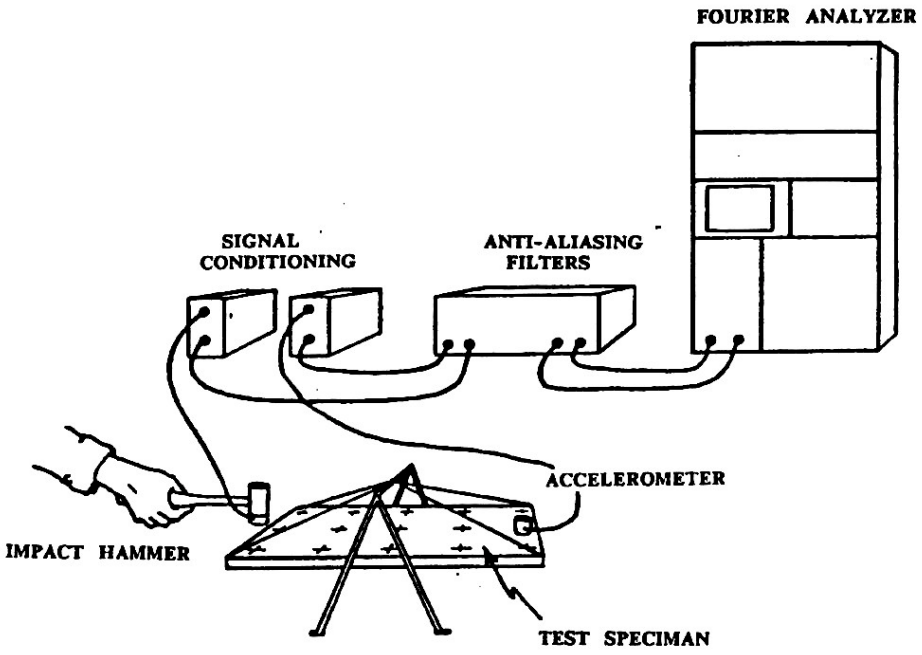

Figure 5-1: Typical experimental set up for an impact hammer test.

The frequency response functions (FRFs) are found using one input (impact) with a number of outputs (acceleration response). Equation 5-2 is the assumed model for the dynamics when using single input FRF estimation:

$$\hat{X}_p - \eta_p = H_{pq} * (\hat{F}_q - \upsilon_q) \qquad \textbf{Eqn 5-2}$$

Where $\hat{F}_q$ is the spectrum of the *q*-th measured input, $\hat{X}_p$ is the spectrum of the *p*-th measured output, H_{pq} is the frequency response function of output *p* with respect to input *q*, υ_p is the spectrum of the input noise, η_p is the spectrum of the output noise, X_p is the theoretical spectrum of the *p*-th output, and F_q is the theoretical spectrum of the *q*-th input. (Allemang, 1999)

Using Equation 5-2, the actual input and output can be found as represented in Equation 5-3,

$$F = \hat{F} - \upsilon$$
$$X = \hat{X} - \eta \qquad \textbf{Eqn 5-3}$$

where *X* and *F* are the actual output and input respectively. In order to minimize the random errors while developing the frequency response functions, averages will be used. This can be achieved by using auto and cross power spectrums to create the following matrices. (Allemang, 1999)

Input/Output Cross Spectra Matrix

$$\mathbf{GXF} = \sum_{1}^{N_{avg}} X_p F_q^* \qquad \textbf{Eqn 5-4}$$

Input Cross Spectra Matrix

$$\mathbf{GFF} = \sum_{1}^{N_{avg}} F_q F_q^* \qquad \textbf{Eqn 5-5}$$

The frequency response functions can be found buy using Equation 5-6

$$\mathbf{H} = \frac{\mathbf{GXF}}{\mathbf{GFF}} \qquad \textbf{Eqn 5-6}$$

From the frequency response functions, the modal parameters can be found by fitting an analytical model to the experimental frequency response functions. There are many techniques for finding the modal parameters from the frequency response functions and these techniques can be found in experimental modal analysis texts such as *Vibrations: Experimental Modal Analysis* by Allemang (1999).

5.2 Procedures for experimental modal analysis of hydraulic test stand structure

The stand was placed on four air shocks, one under each corner of the base plate, as seen in Figure 5-2. Then the air shocks were filled with air so that the top of the base plate is 7 ½" above the ground. This isolates the movements of the test stand from the movements of the building, and approximates a free-free boundary condition.

Figure 5-2: Structure set up.

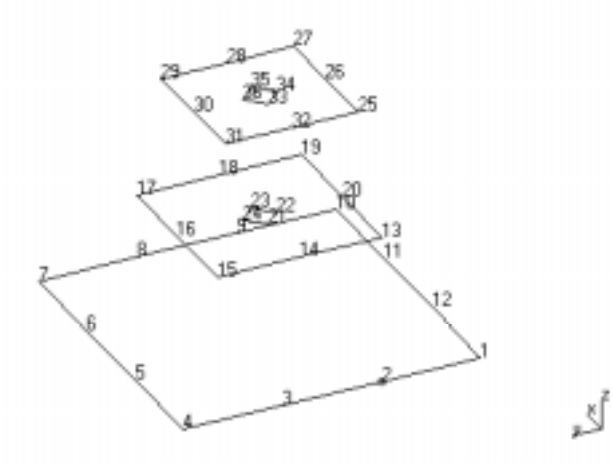

Figure 5-3: The outline of the three plates. The accelerometers sit on points 1, 15 and 27.

One point on each plate (Plate #1, Plate #2, and Plate #3) was chosen to mount three, single-axis accelerometers (oriented in the x, y, and z directions) and a coordinate system was picked. Figure 5-3 displays the accelerometer mounting and coordinate system used. The origin of the coordinate system is placed at the accelerometer mounting on Plate #1. The positive x-direction is along the edge of Plate #1 parallel to the I-beams. The positive y-direction is along the edge of Plate #1 perpendicular to the I-beams. The positive z-direction is perpendicular to the plate, with increasing elevation.

Next, the impact points were chosen. Plate #1 has four impact points on each side, as seen in Figure 5-4(a). Plate #2 has three impact points on each side and four placed 2” from the center, as seen in Figure 5-4(b). Plate #3 has three impact points on each side and four placed 2” from the center, as seen in Figure 5-4(c).

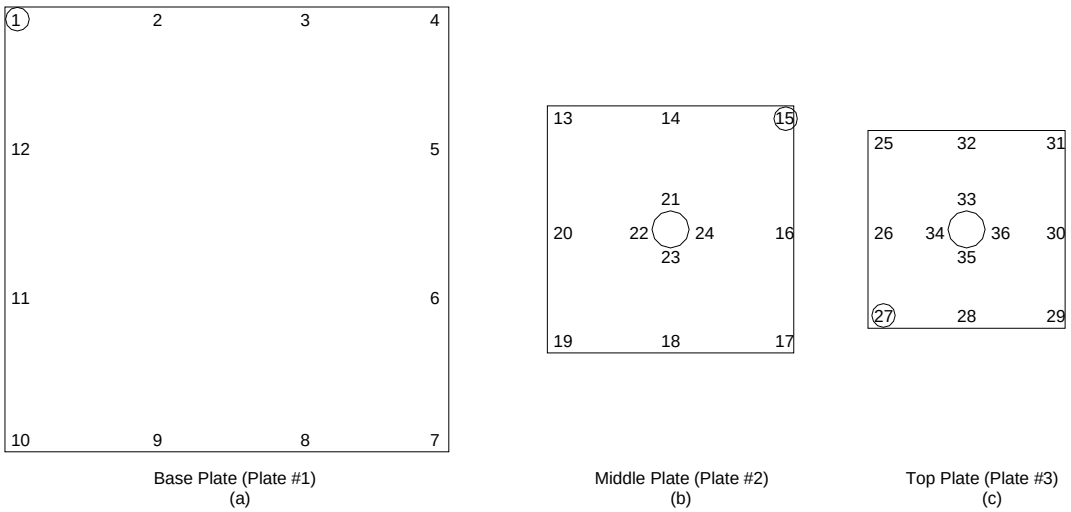

Figure 5-4: Impact points on each plate, (a) is plate #1, (b) is plate #2, and (c) is plate #3. The circled points are where the accelerometers were placed.

Each point was numbered as seen in Figure 5-4 (a-c). Using an instrumented impact hammer (PCB Model II) with a rubber damping tip generates a frequency range of 0-250 Hz and a rollover of less than 20 db in amplitude over this frequency range. An impact test was performed in each possible direction at each point. All corner points had an impact test in the x, y, and z directions. The points at the sides of the plates had impact tests in the z-direction and perpendicular to the edge. The eight points in the middle of Plate #2 and Plate #3 had impact tests performed in the z-direction only. To reduce the error of a skew impact, five impacts were taken and averaged for each point and direction. The force and exponential window was utilized to reduce measurement error and leakage errors as well.

The same test was completed on the structure of the test stand, with the 2 ½" hydraulic cylinder attached except each point was only excited in the z-direction

with the exception of points 1, 19, and 31 which were excited in all three directions. Figure 5-5 shows the excitation of point 5 in the –z direction with the cylinder attached to the structure.

Figure 5-5: The vibrations test set up with the 2 ½" cylinder in place in the stand.

5.3 Analysis and Results

In total, 73 impact tests were performed on the structure itself and 45 impact tests were performed on the structure with the hydraulic cylinder attached. The raw data was then loaded into the X-Modal II software (University of Cincinnati, SDRL, 2000) to be analyzed using the Complex Mode Indication Function (CMIF). The natural frequencies and their corresponding modes were found.

For the structure alone, there were 5 rigid body modes that will change with the boundary conditions. The first flexible mode for the structure alone was found at

61.25 Hz, the next at 109.85 Hz. Figure 5-6 displays the FRF for the input at point 21 in the –z direction and the output at point 15 in the +z direction.

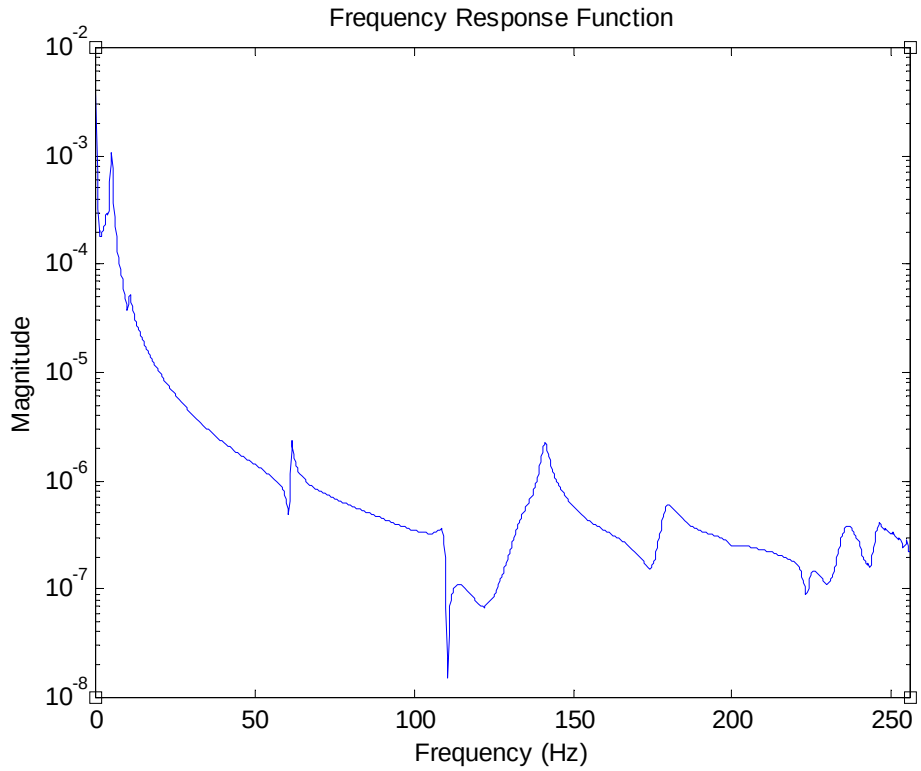

Figure 5-6: The FRF of the test stand structure alone with an input at point 21 in the –z direction and the output at point 15 in the +z direction.

The above FRF shows a strong effect of the 61 Hz mode at the attachment point of the cylinders, but not a large effect at 111 Hz. Figure 5-7 is the FRF with the input at point 22 in the –z direction and the output at point 15 in the –y direction. This FRF shows a strong effect of the mode at 111 Hz. These two FRFs indicate that the two modes at 61 Hz and 111 Hz may have an effect on the hydraulic cylinder when it is attached to the stand.

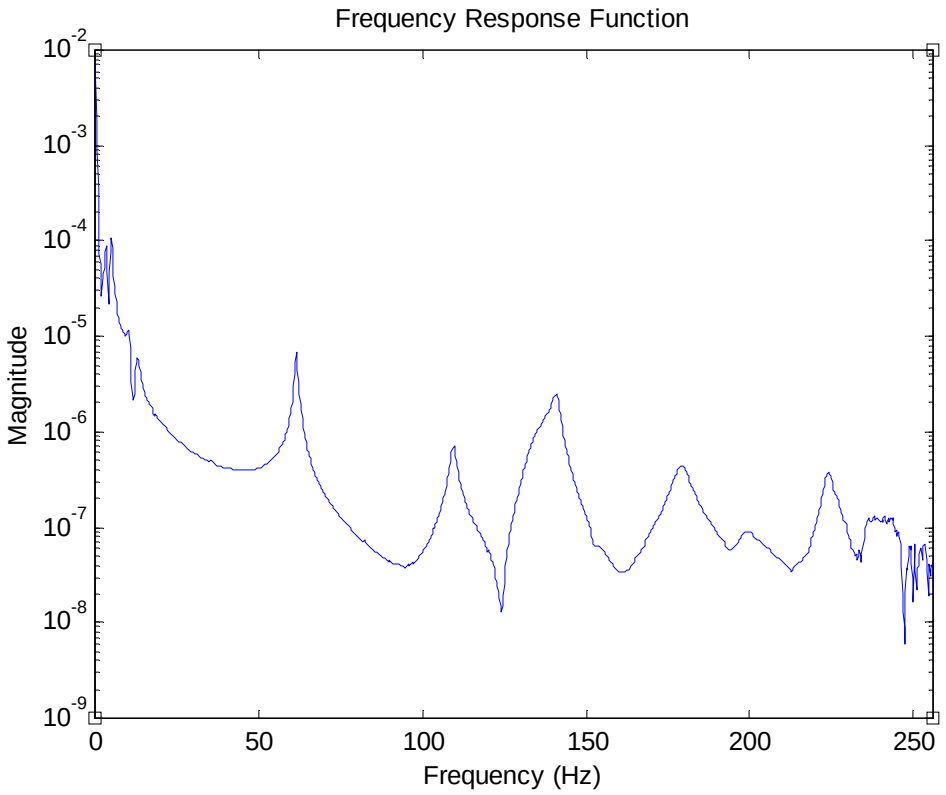

Figure 5-7: The FRF at 109.85 for the test stand structure alone.

Using X-Modal II, the modes of these two frequencies have been animated and Figures 5-8 and 5-9 represent snapshots of the modes at 61 and 109 Hz at their maximum deformation. Note that point 2 was either a node or was incorrectly inputted into the model, therefore, it does not move at all.

The first flexible mode looks to be a bending of the I-beam web in the y-direction, because plate #2 and #3 move in parallel, but are not in phase with the movement of plate #1. Extra support such as welding pipes or gussets between the flanges of the I-beams may increase the stiffness of this area, in effect raising the frequency of the first flexible mode if needed.

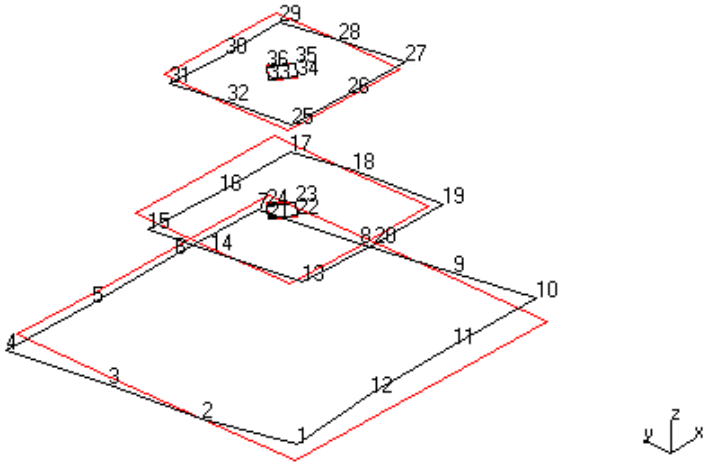

Figure 5-8: Maximum deformation for the mode at 61.25 Hz for the test stand structure itself.

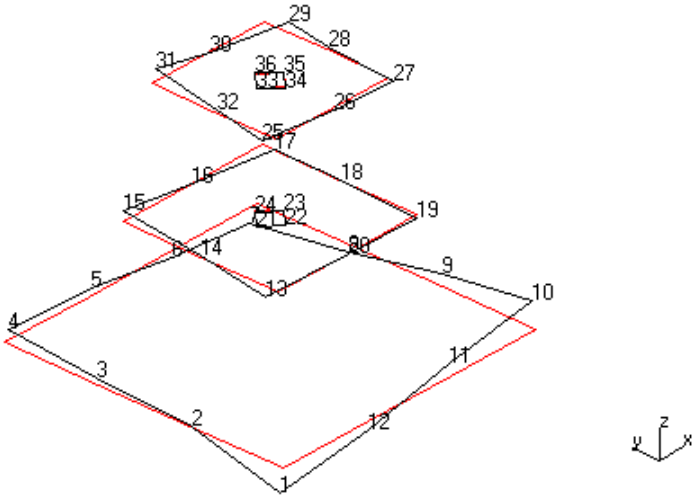

Figure 5-9: Maximum deformation for the mode at 109.85 Hz for the test stand structure itself.

For the test stand with the cylinder attached, there were 5 rigid body modes found with the first two flexible modes being found at 61 Hz and 111 Hz. These modes and frequencies are important because they become apparent at the points where the cylinder is attached. Figure 5-10 is the FRF for the input at point 22 in the -z direction and the output at point 15 in the +z direction.

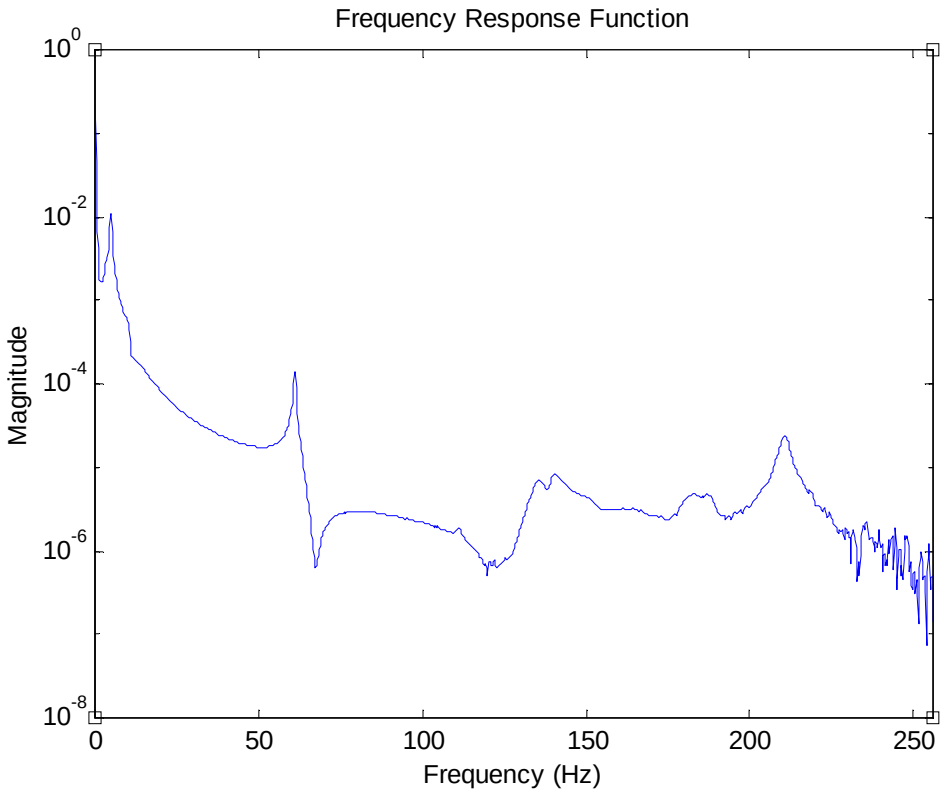

Figure 5-10: The FRF for the test stand structure with the cylinder attached for the input at point 22 in the –z direction and the output at point 15 in the +z direction.

Note that the mode at 61 Hz is very prevalent, and the mode at 111 Hz is not very prevalent in this FRF. Figure 5-11 is the FRF for the input at point 24 in the –y direction and the output at point 15 in the x direction. This particular input was done on the mounting plate of the cylinder. Note that the mode at 111 Hz has become reasonably prevalent, indicating that this frequency may effect the hydraulic system.

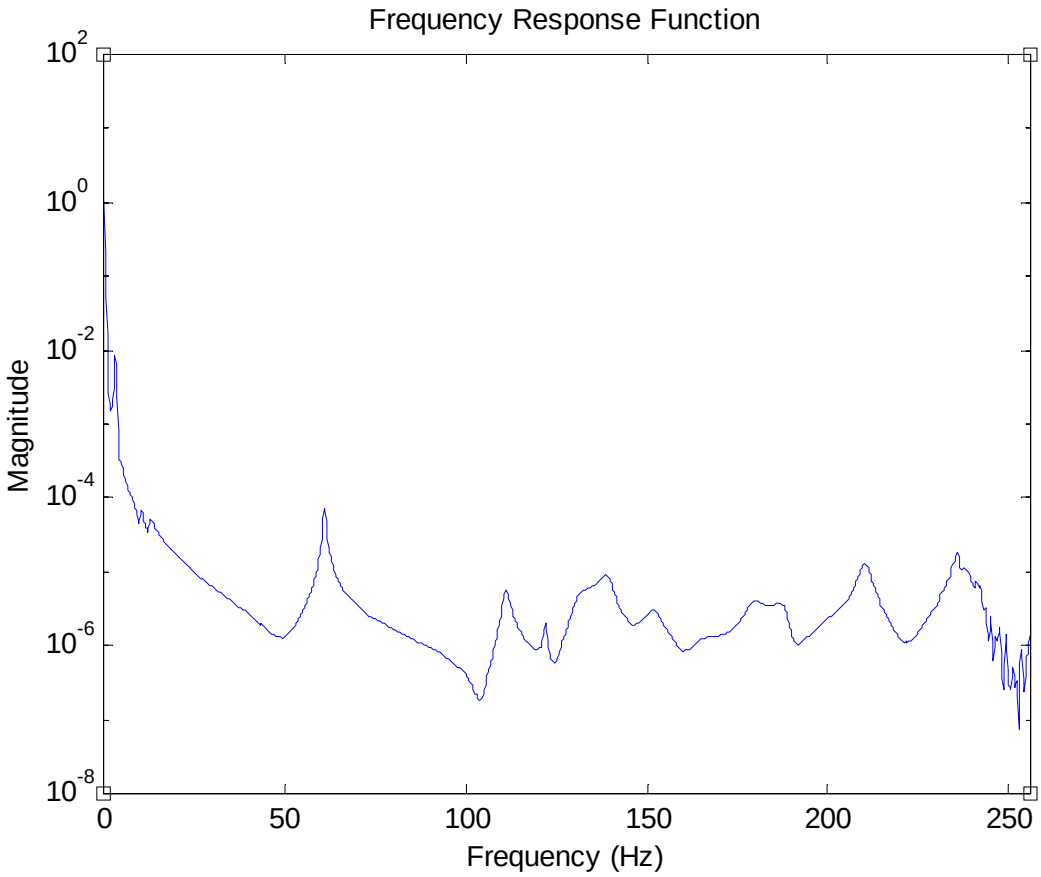

Figure 5-11: The FRF at 111 Hz for the test stand with the cylinder attached.

Using X-Modal II, the modes of these two frequencies have been animated and Figures 5-12 and 5-13 represent snapshots of the modes at 61 and 111 Hz at their maximum deformation. Note that point 2 was incorrectly inputted into the model, therefore, it does not move at all.

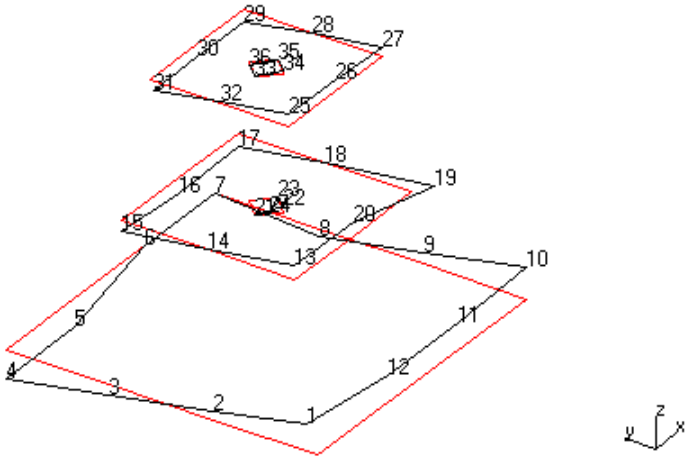

Figure 5-12: The modal deformation of the test stand structure with the cylinder attached, at 61 Hz.

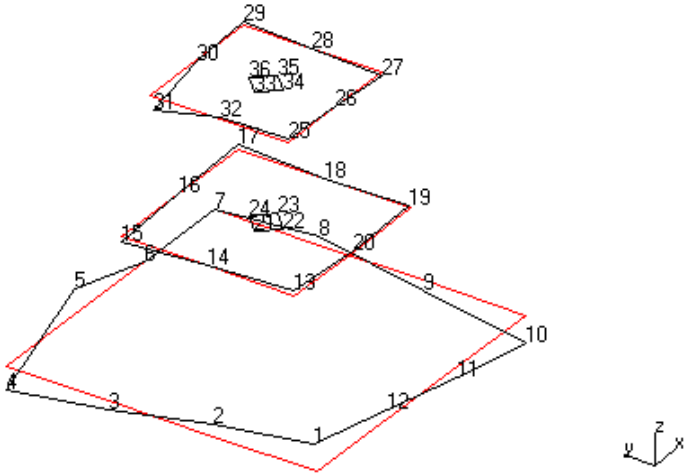

Figure 5-13: The modal deformation of the test stand structure with the cylinder attached, at 111 Hz.

Again, the first flexible mode looks to be a bending of the I-beam web in the y-direction, because plate #2 and #3 move in parallel, but are not in phase with the movement of plate #1, and extra support in the I-beam such as welding pipes,

gussets or brackets between the flanges of the I-beams may increase the stiffness of this area, in effect raising the frequency of the first flexible mode if needed.

The reciprocity between the z-direction inputs and outputs was very good, while the reciprocity between the x or y-direction inputs ands z-direction outputs was very poor. This is to be expected because the stiffness in the x and y-directions is much greater that the stiffness in the z-direction. If the impact direction was not contained within the x-y plane, the small force in the z-direction will greatly affect the test data.

5.4 Additional experimental modal analysis

After an in depth discussion with Prof. Allemang, Prof. Berger and Prof. Thomson, it was concluded that an additional impact test, with boundary conditions that approximated a fixed plate condition, needed to be performed. This additional testing should make certain that the natural frequencies of the structure with boundary conditions near that of the structure during the non-linear testing, will be out of the 0-50 Hz frequency range of the servo-valve.

The air shocks were removed from under the structure and replaced with a thin rubber mat. This changed the boundary conditions from approximating a free-free condition to a fixed plate condition, with the rubber mat reducing the amount of error due to floor movement. The structure was then impacted in the –z-direction at all of the outside points on the top two plates and points 22, 24, 34,

and 36 in the center of the top two plates. Each point was also impacted in the x-y plane as well.

The changed boundary conditions revealed natural frequencies at 21, 28, 39, and 49 Hz. These can be seen in the following two figures.

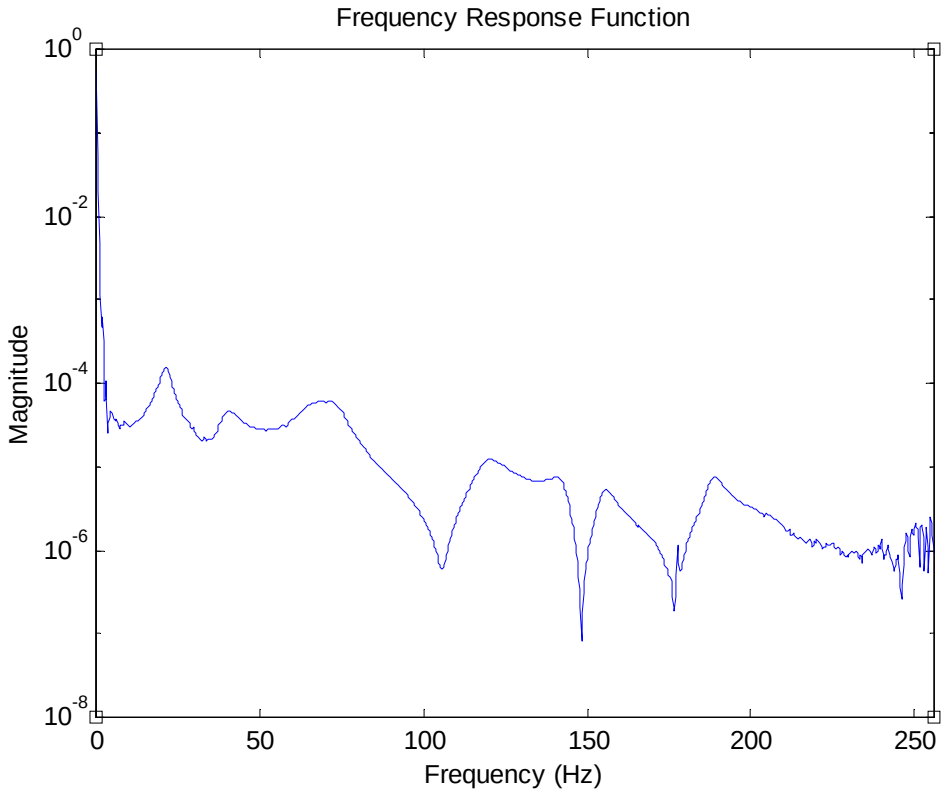

Figure 5-14: The FRF of the hydraulic test stand structure with the cylinder attached and resting on a thin rubber mat with the input at point 20 in the –z-direction and the output at point 15 in the +z-direction.

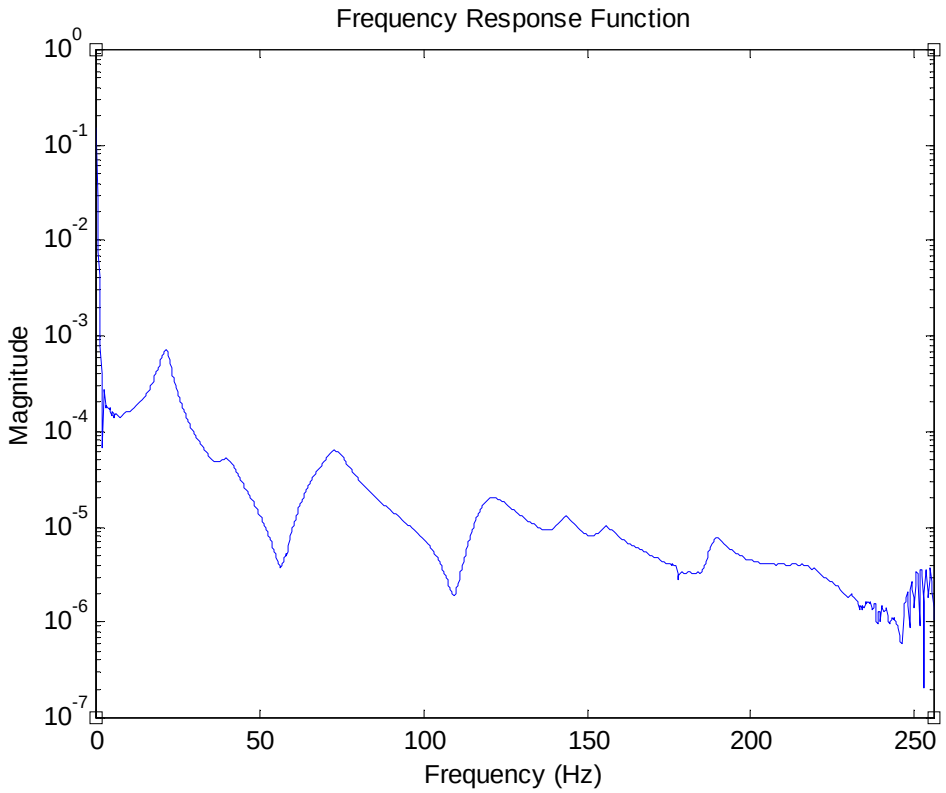

Figure 5-15: The FRF of the hydraulic test stand structure with the cylinder attached and resting on a thin rubber mat with the input at point 20 in the –z-direction and the output at point 15 in the +y-direction.

These four natural frequencies are within the 0-50 Hz bandwidth of a commercially available servo-valve, therefore the modes were animated with the aid of the X-Modal II software (University of Cincinnati, SDRL 1999). From the animations it was observed that the top two plates moved, in unison, from side to side in the y-direction at the natural frequency of 21 Hz, the plates rotated within the xy-plane at the natural frequencies of 28 Hz and 39 Hz, and the plates moved, in unison, from side to side in the x-direction at the frequency of 49 Hz. These four modes appear move the top two plates and the hydraulic system in unison, within the xy-plane so they should not disrupt the hydraulic system.

The testing also found natural frequencies at 67 Hz, 89 Hz, and 121 Hz, but these are not within the bandwidth of the servo-valve so they should not affect the hydraulic system dynamics.

5.5 Conclusion

The experimental modal analysis concluded that there are modes near 61 Hz and 110 Hz. With the addition of a cylinder the mode at 61 Hz did not change, and the mode near 110 changed slightly from 109 to 111 Hz. This shows that the cylinder attachment has little effect on the mode at 61 Hz, but may have some effect at the mode near 110 Hz.

The first mode at 61 Hz looks as if there is bending in the I-beam web with or without the cylinder attachment. Assuming the mode at 61 Hz is a flexible mode, the I-beams can be stiffened using baffles or welding in piping between the flanges of the I-beams. The mode near 110 Hz looks as if it is the flexing of Plate #1 and should become irrelevant if the test stand is fixed to the floor or seismic mass.

When looking at the animation of the mode at 61 Hz, the three plates look like they are close to moving together. Further testing is needed to completely verify that this mode is indeed a flexible mode and the effect of the addition of the hydraulic cylinder.

One of the design constraints for the future use of the stand for non-linear dynamic testing is the bandwidth of a commercially available servo-valve. The maximum bandwidth for a commercially available servo-valve is 50 Hz to stay

reasonably economical. Therefore these two modes are outside the frequency range at which the hydraulic system can operate, so they should not affect the hydraulic system.

Chapter 6: Friction characterization of the hydraulic actuator sealing system

The friction phenomenon has been difficult to understand using analytical means, and is generally defined empirically. The extent of the zero velocity regime and the transition from the zero velocity to a non-zero velocity or low velocity dynamics, have been examined and are presented in this chapter. Testing of breakaway pressures and low velocity dynamics was performed on two cylinders, one with a 3-1/4” bore and the other with a 2-1/2” bore size, both having low friction seals and 7” strokes. Before getting into the testing procedures, a review of friction and the relation of friction to hydraulic systems is necessary.

6.1 Definition of friction

Friction is an integral part of life. This phenomenon has been manipulated since the beginning of human existence, reducing friction when it is wasteful and increasing friction when it is beneficial. In most situations, friction is unproductive and needs to be lessened; though, it is essential in daily life, making things such as braking, weaving, gripping of tires (on cars), internal combustion engines, friction cutting, and fastening possible. Lubrication to reduce friction has been utilized since early times. The use of animal fats and oils as lubricants is depicted in ancient temple paintings and Egyptian tombs. (Seireg, 1980)

Friction can be divided into four regimes: dry, boundary, elastohydrodynamic, and hydrodynamic. Dry friction theory describes the friction loads between two clean, dry surfaces where the cleanliness of the surfaces becomes the

dominating factor influencing the frictional resistances, as seen in Figure 6-1. Boundary friction theory describes the frictional resistance when the surfaces are between the dry and the elastohydrodynamic regimes, as seen in Figure 6-2. The elastohydrodynamic theory describes the frictional resistances with small lubrication films between two surfaces so that the surfaces are still in partial contact with each other, as seen in Figure 6-3. Hydrodynamic theory describes the frictional resistances when there is a thick lubrication film between two surfaces and no contact between the two surfaces, as seen in Figure 6-4. Osborne Reynolds found that the viscosity and thickness of lubrication film are the major parameters that define hydrodynamic friction, not the density as previously assumed (Seireg, 1980). Dry friction has the most frictional resistance, while the resistance lessens as the amount of lubrication increases resulting in hydrodynamic friction having the least resistance.

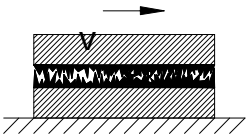

Figure 6-1: Dry Friction.

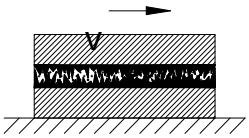

Figure 6-2: Boundary Layer Friction.

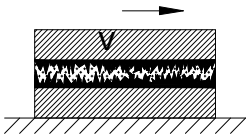

Figure 6-3: Elastohydro-dynamic friction.

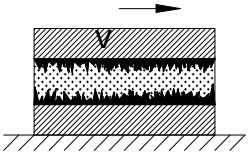

Figure 6-4: Hydrodynamic Friction.

6.2 Friction in hydraulic actuators

In hydraulic actuators, friction is found in two forms - the friction due to the viscous fluid flow itself and the sliding friction found where the seals contact the metal surfaces of the cylinder or shaft. The friction due to viscous fluid flow in the actuator is significantly smaller than the friction due to the seals so the fluid flow

friction in the actuator will be considered negligible and the focus will be placed on the seal friction.

The friction forces relating to the sliding of the seals are a function of the piston velocity. In general the friction is simplified to be Coulomb friction as seen in Figure 6-5. As depicted, Coulomb friction is non-linear, dependent on the velocity direction and can be split into two regimes. The first regime covers the operation space where velocity is zero and the second regime encompasses the remainder of the operation space when velocity is not equal to zero.

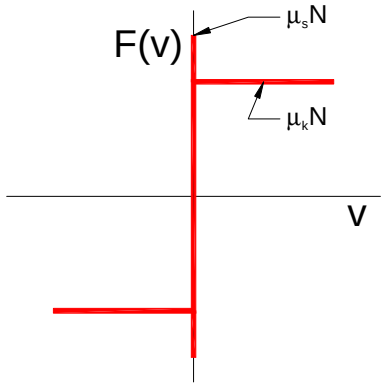

Figure 6-5: The Coulomb friction model

In Coulomb friction, when the velocity is zero the actual friction force is equal to the force acting on the piston as long as the static threshold ($\mu_s N$) value is not exceeded. The equations below express the actual friction force when the velocity is zero,

$$F_p = F_f \leq \mu_s N \quad \text{when} \quad \dot{x} = 0 \qquad \textbf{Eqn 6-1}$$

where F_f is the actual friction force (lb_f), F_p is the force acting on the piston (lbf), μ_s is the static friction coefficient, and N is the force acting normal to the surfaces in contact (lb_f). When the actual friction force exceeds the static threshold, breakaway occurs, and the velocity becomes non-zero. (Serway, 1994)

When the velocity is non-zero the friction force is proportional to the normal force by the dynamic friction coefficient, μ_k, as shown in the equation below.

$$F_f = \mu_k N \quad \text{when} \quad \dot{x} \neq 0 \qquad \textbf{Eqn 6-2}$$

The two friction coefficients, μ_s and μ_k, are nearly impossible to define analytically because they encompass the physical states and material characteristics of the contact area. Variables such as roughness of each surface, viscosity of lubrication, thickness of lubrication film, amount of contact area between the two surfaces, and pliability of each surface are just a few issues that must be taken into consideration when defining the friction coefficients. In a hydraulic system, these variables can vary from component to component, and application to application. The length of time a cylinder sits or runs can also be a factor in the friction. Because of the complexity, the friction coefficients are normally found empirically.

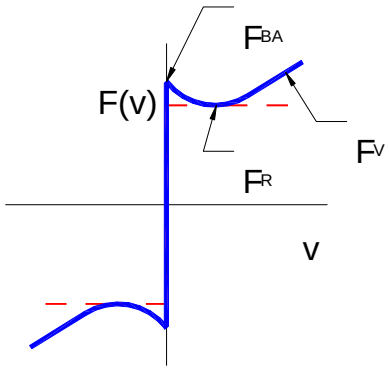

Figure 6-6: Stribeck Curve a better representation of friction in a hydraulic system.

In reality, the Coulomb friction representation is not a very accurate model for the friction forces in a hydraulic actuator. Figure 6-6, also known as a Stribeck curve, gives a better representation of the friction in general. The friction can be divided into three components: breakaway friction (F_{BA}), running friction (F_R), and viscous friction (F_V). The breakaway friction mimics the zero velocity range of Coulomb friction. The running friction accounts for the dynamic friction, and mimics the non-zero velocity regime of Coulomb friction. As the system transitions from breakaway

friction to running friction, it does not actually happen instantaneously, instead the drop occurs over a short amount of time. The friction found in the hydraulic cylinder varies from Coulomb friction with the introduction of the viscous friction. The viscous friction model introduces the friction associated with the lubrication film. In other words, as the velocity increases, the friction force increases as well, normally it is the square or cube of the velocity (Johnson, 1995). The values of each friction component can be found experimentally.

Highly accurate characterization of friction properties requires high precision measurements, and is beyond the scope of this thesis.

6.3 Friction and seals

When dealing with hydraulic control systems, it is preferred to keep the fluid contained within the system. Containment is accomplished by using seals on areas where a clearance is needed for movement. In double acting hydraulic cylinders, there are two such areas: the piston land separating the two volumes of oil within the piston, and the rod seal where the rod extends out of the cylinder housing. Figure 6-7 is a cross section of a hydraulic cylinder and shows both sealing surfaces found in a cylinder (Muller, 1998) (Horve, 1996).

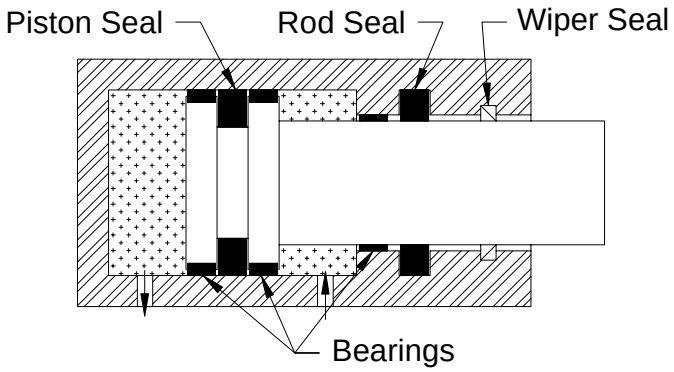

Figure 6-7: Typical sealing elements in a hydraulic actuator.

The lubrication between the seals and contact surface governs the magnitude of the sliding friction forces found in hydraulic cylinders. Once the seal area reaches a hydrodynamic state, the friction is minimal. This requires some leakage, but to achieve a hydrodynamic state, a lubrication film thickness of only 1-2 μm is needed. This can be achieved by correctly designing the seals (Muller, 1998).

Many standard hydraulic cylinders use U-cup elastomeric seals, as seen in Figure 6-8, for rod seals because they do a good job of sealing and are economical. The geometry allows for a good seal, as well as good lubrication of the sealing surface due to the chamfered edge. The elastomeric seals have some drawbacks. These seals have a tendency to create a stick-slip situation within the cylinder, causing the rod to jump as the working force exceeds the static friction force. This can also cause severe vibration that can be amplified if the stick-slip frequency is in resonance with the natural mode of the system. The elastomeric materials also

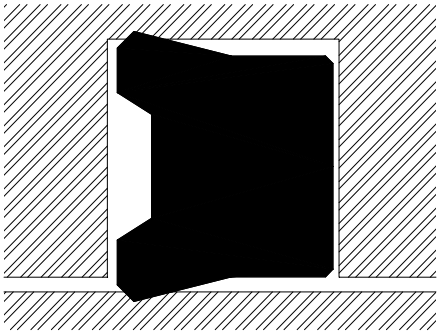

Figure 6-8: U-cup elastomeric seal profile.

cannot handle temperatures exceeding 80^{o}C, and velocities exceeding 30 m/min due to friction heat (Muller,1998).

For precise positioning systems stick-slip is intolerable, so the seals are made of harder polymers such as Teflon and PTFE using brass to reinforce them. These polymers must be molded and machined, causing inherent microscopic crevices in the surface acting as lubricant pools that can reduce pockets of high static friction quickly. The PTFE seals are not normally U-cups because the material cannot sustain a radial preload as elastomeric material can. Instead, the PTFE seals are used in conjunction with metals and elastomeric O-rings. The elastomeric O-rings are used so that there is a preload on the seal. Figure 6-9 illustrates three different configurations for PTFE seals. Figure 6-9 (a) shows a preloaded elastomeric o-ring behind a block PTFE seal. This configuration is commonly found in the piston seals. Figure 6-9 (b) uses a step PTFE seal instead of a block seal. This step seal configuration is used for the rod seals, where the

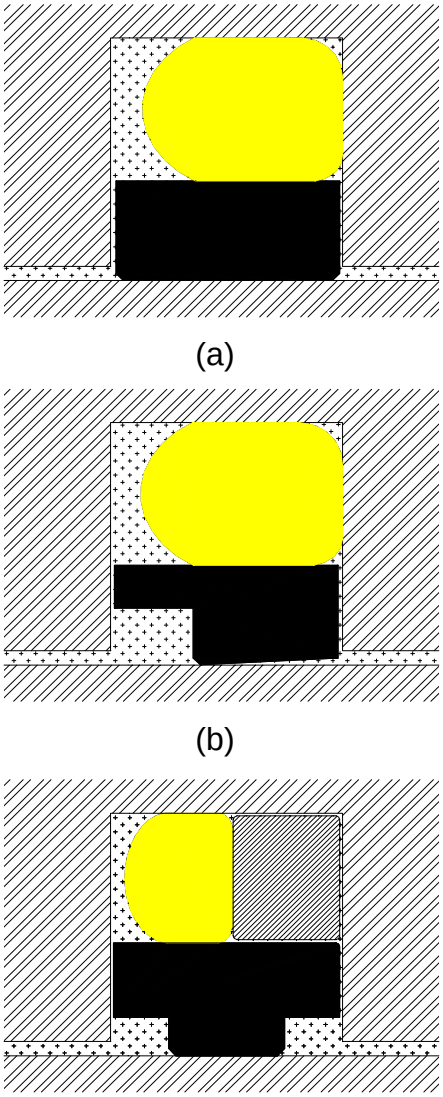

Figure 6-9: PTFE seal configurations.

smaller part of the PTFE seal is on the internal side of the seal, and the thick part of the PTFE seal is on the external part of the seal. Figure 6-9 (c) includes a metal back-up ring as well as using a T configuration for the PTFE. The metal back-up ring helps keep pressure on the o-ring reducing the leakage past the seal. (Muller, 1998)

Leakage is most important for the rod seal, but it is also important to reduce the amount of foreign objects entering the system such as dirt and ice during the retraction of the cylinder as well as reducing the amount of fluid leaving the system during the extension of the cylinder. In addition to the rod seal, often there is a wiper seal, as depicted in Figure 6-7, that “wipes” the rod clean of debris, leaving a small film of lubricant on the retraction of the cylinder. The piston seals are often o-rings because leakage across the piston is not detrimental to the system; this leakage actually damps the system. (Muller, 1998)

The hydraulic system design being considered has low friction seals. These sealing mechanism uses bronze-filled PTFE for low friction, in conjunction with elastomer expanders to preload the seal. Figure 6-10 depicts the sealing configurations used on the test cylinders.

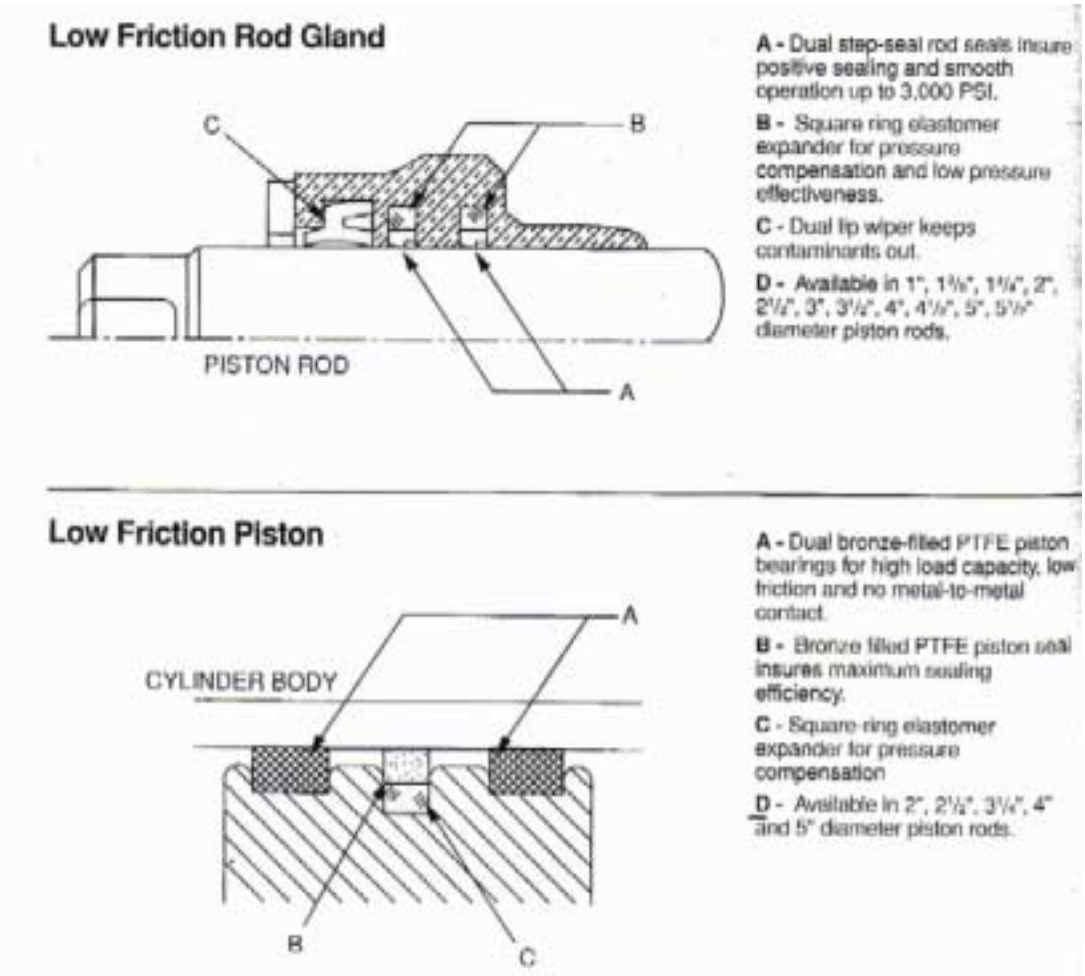

Figure 6-10: Low friction sealing configuration of the Parker 3L cylinders (courtesy of Parker Hannifin).

6.4 Testing procedures for breakaway pressures

When the net pressure force acting on the piston overcomes the static friction force, the piston begins to move, or breaks away. The pressure gradient across the piston at which this breaking away occurs is termed the breakaway pressure of the actuator. The breakaway pressure can be found by measuring the pressure at each port of the cylinder when the piston starts to move. Figure 6-11 is the basic hydraulic circuit used in these experiments to determine the breakaway pressure.

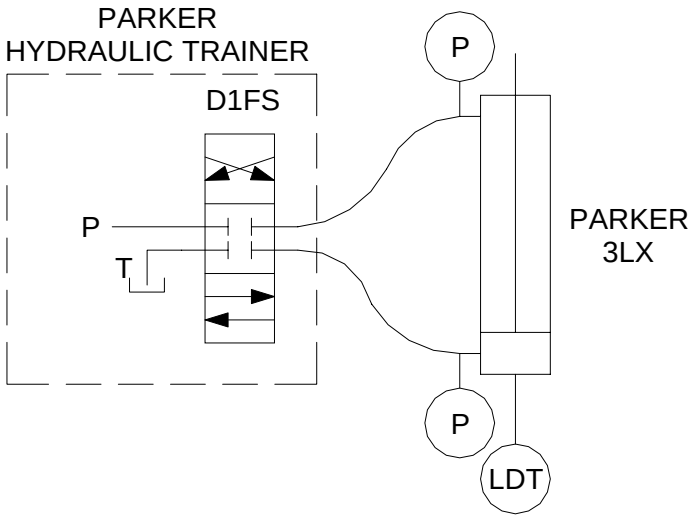

Figure 6-11: Hydraulic circuit used in breakaway pressure testing.

For the following experiments, 3-¼" and 2-½" bore size Parker 3LX cylinders, with low friction seals were tested, fixed to the Hydraulic Test Stand, as seen in Figure 1-2. Both cylinders contain an internal linear displacement transducer (LDT) used to track the position of the piston. PCB Piezotronics DCS Series 1500 Pressure sensors were attached at the ports of each cylinder. The Parker Industrial Hydraulic Trainer (IHT) contains the power unit and proportional valve (D1FS series valve). Hose with quick disconnects was used to connect the Parker IHT assembly with the Cylinder assembly. The signals were all sent to the Zonic – Medallion (model 2808) data analyzer for data collection with the input signal connected to Channel 1, the LDT connected to Channel 2, the rod side pressure transducer connected to Channel 3, and the LDT side pressure transducer connected to Channel 4.

Each cylinder's breakaway pressure is tested over the operating pressure range of 300 to 500 psi at an interval of 50 psi. The following steps were performed at each pressure setting.

1. The valve control board is set for open loop and an external input. The external input is set to a +/- 3V square wave at 0.2 Hz.

2. The system is brought to the appropriate operating pressure.

3. The cylinder is stroked fully 5 times to allow good lubrication of the sealing surfaces.

4. The Medallion records the pressures, piston position, and input signal for 16 seconds.

5. The entire system is allowed to reach atmospheric pressure.

6. Steps 1 through 5 are repeated FIVE times.

7. The valve control board is set for open loop with an external input of a triangular wave at +/- 5 V at 0.2 Hz.

8. Steps 2 through 5 are repeated FIVE times.

6.5 Analysis and results

With the low friction seals, it is expected that the breakaway pressure will not vary greatly due to the varying operating system pressure, because the seal configuration does not rely on the volume pressure to regulate the sealing force.

In the experiment, the pressure on both sides of the piston, the piston position and the input signal were recorded. As an example, Figure 6-12 shows the raw data for a 2 ½" bore cylinder being run at 500 psi with a 3.5V amplitude square wave being sent to the proportional valve as a control signal.

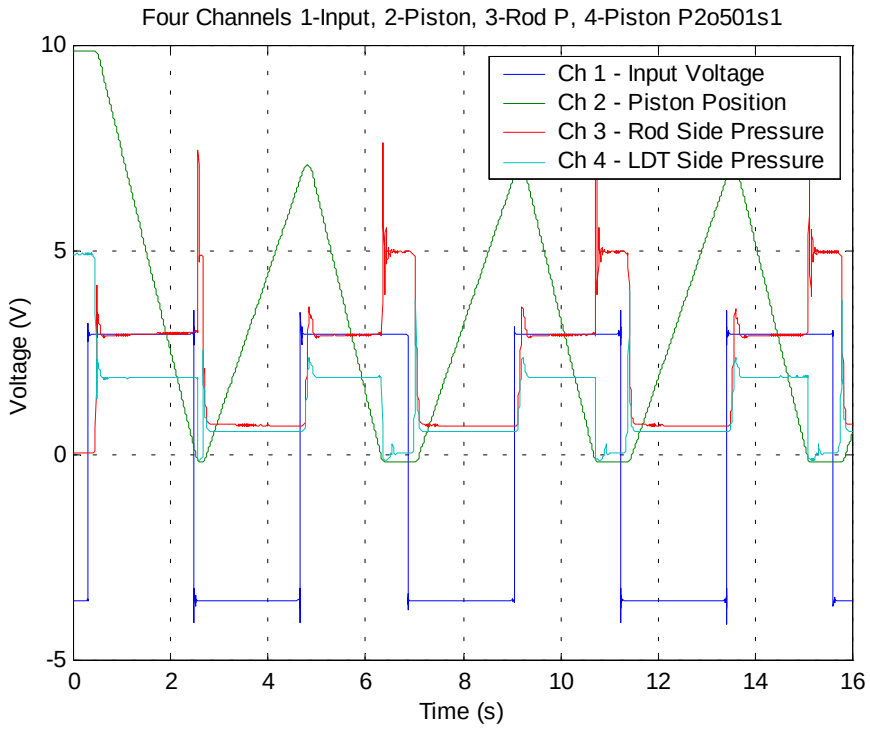

Figure 6-12: Data output for a 2 ½" Cylinder at an operating pressure of 500 psi, and a +/- 3.5V square wave input.

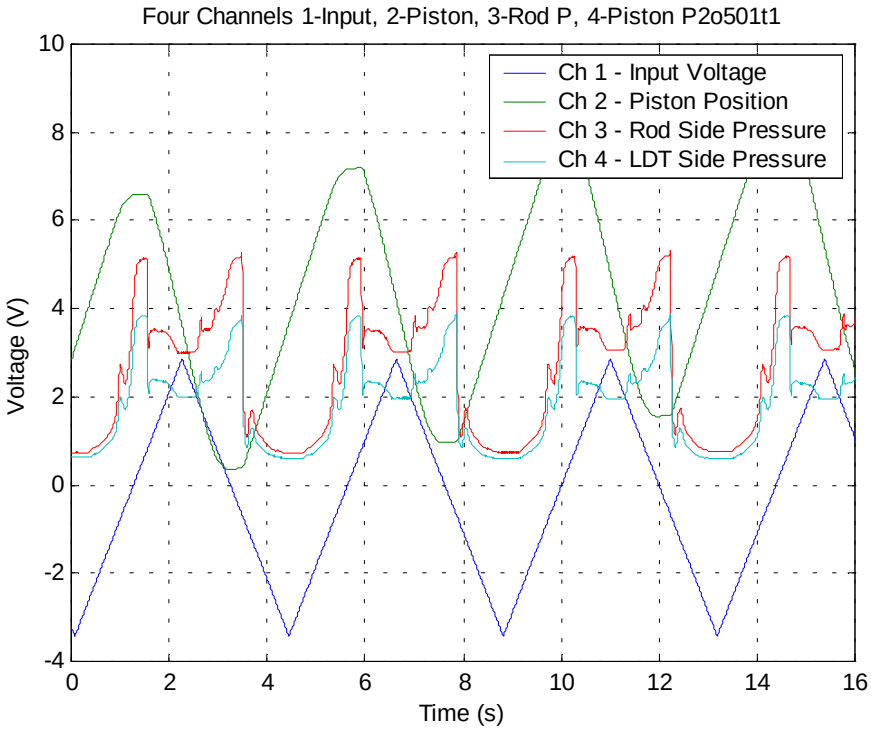

Figure 6-13: Data output for a 2 ½" Cylinder at an operating pressure of 500 psi, and a +/- 3.5V triangular wave input.

Figure 6-13 shows the raw data for the same system as seen in Figure 6-12 except there is a triangular input wave. The raw data was converted from volts to the appropriate units: psi for pressures, and inches for the cylinder position. Then the data was used to find the pressure drop across the piston by subtracting the pressure on the rod side of the cylinder (P_{Ch3}) from the pressure on the LDT side of the cylinder (P_{Ch4}) as shown in the following equation:

$$\Delta P = P_{Ch4} - P_{Ch3} \qquad \textbf{Eqn 6-3}$$

Due to the unequal areas on each side of the piston, the pressure drop varies due to the direction the cylinder is moving. The force across the piston (ΔF) was then found as shown in Equation 6-4:

$$\Delta F = P_{Ch4}(A_{piston} - A_{LDT}) - P_{Ch3}(A_{piston} - A_{Rod}) \qquad \textbf{Eqn 6-4}$$

where A_{piston} is the cross sectional area of the piston, A_{LDT} is the cross sectional area of the LDT rod, and A_{Rod} is the area of the piston rod. The pressure drops and forces across the piston were graphed with the piston position to find the breakaway pressures and forces for each set of data. Figures 6-14 and 6-15 are examples of these graphs. Figure 6-14 displays the pressure drop and piston position of the 3 ¼" bore cylinder operating at a pressure of 450 psi and having a square wave input, while Figure 6-15 presents the force across the piston and piston position of the 3 ¼" bore cylinder operating a pressure of 450 psi and having a triangular wave input.

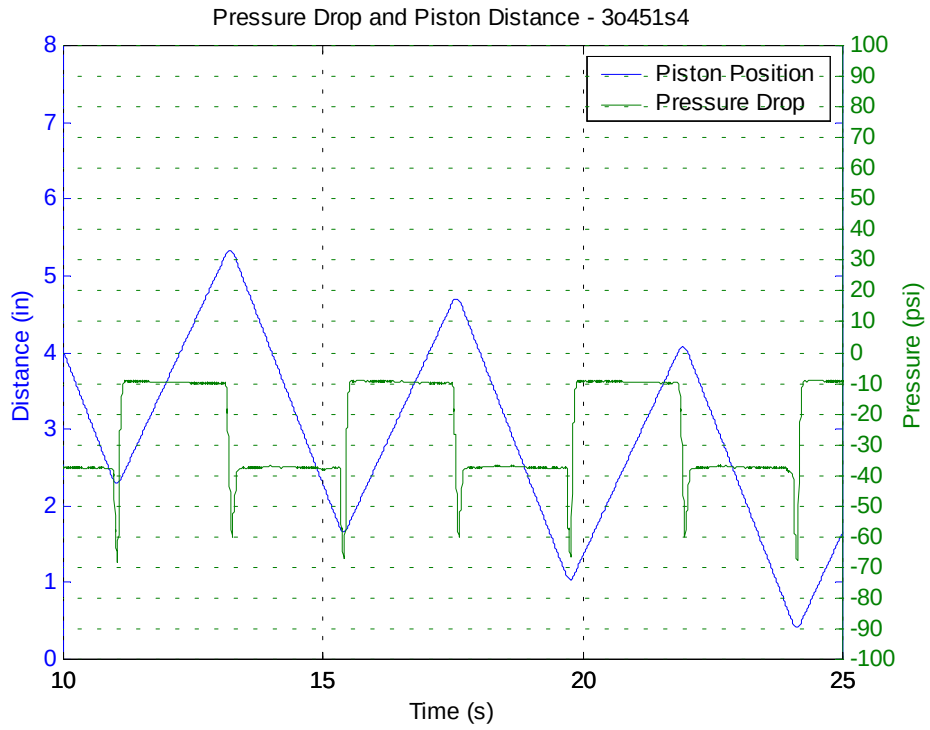

Figure 6-14: Pressure drop and piston position for a 3 ¼" bore cylinder operating at 450 psi with a square wave input to the proportional valve.

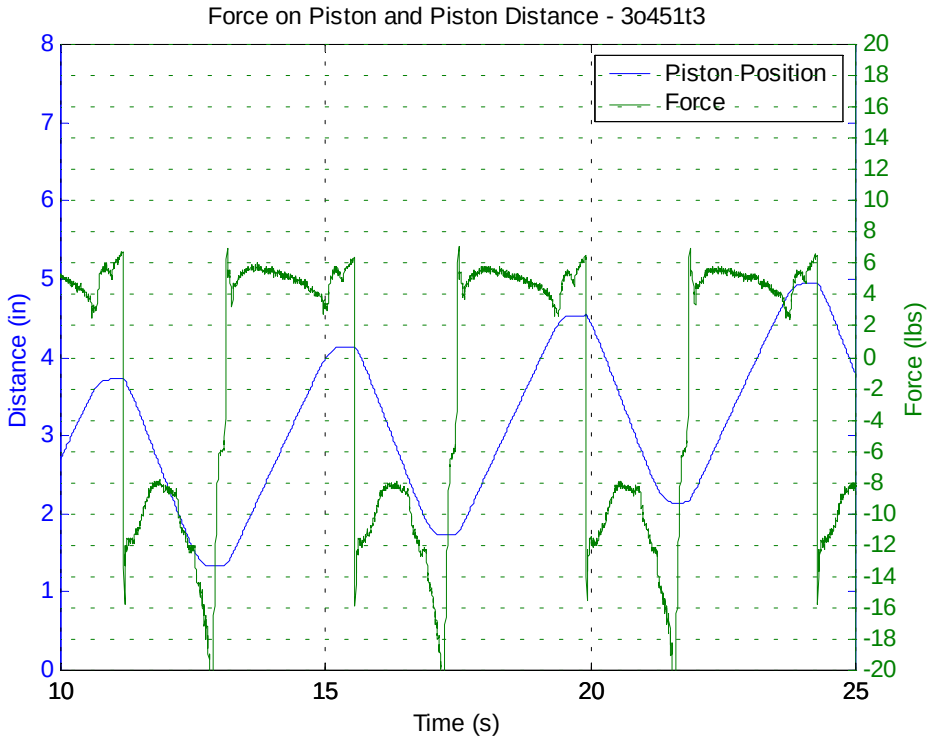

Figure 6-15: Force across the piston and piston position versus time, for a 3 ¼" bore cylinder operating at 450 psi and the proportional valve receiving a triangular wave input.

The breakaway pressure and forces occur where the piston stops to change directions and are depicted as spikes in Figures 6-14 and 6-15. The breakaway points from all of the data sets were assembled to see how uniform the breakaway pressures and forces were across the data sets. The following figures show the relationships between the breakaway pressure and forces to the operating pressure, the piston diameter, the direction of movement, the input type (whether the wave is triangular or square), and the piston position.

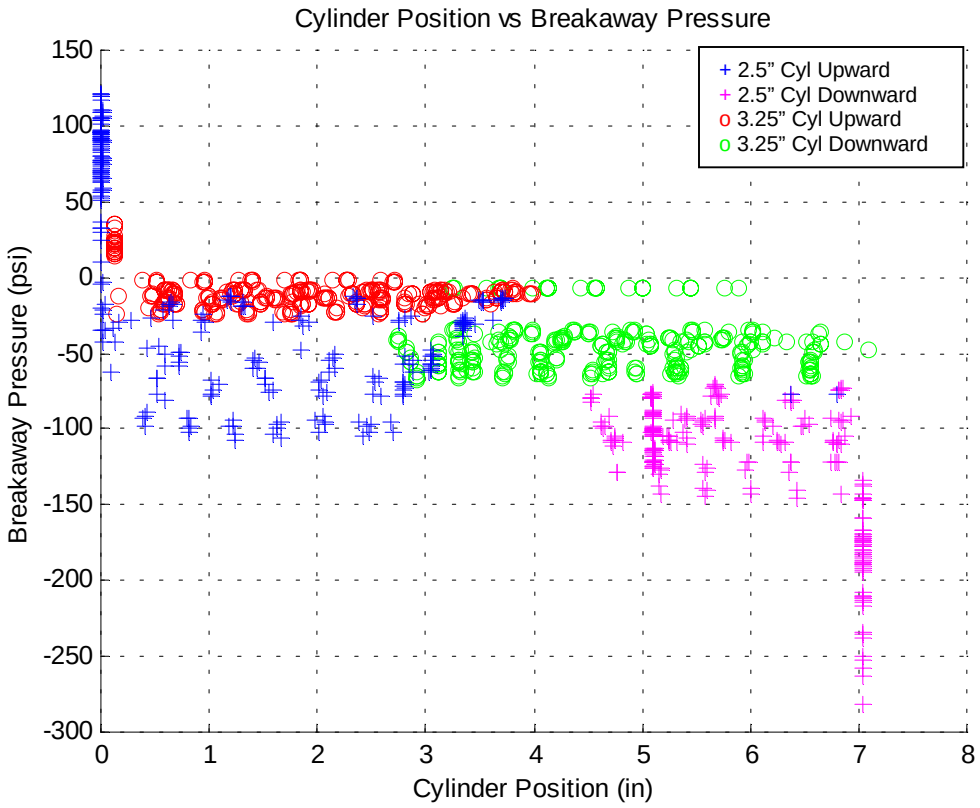

Figure 6-16: The cylinder position versus breakaway pressure delineating between the sized of the cylinder and the direction in which the piston is traveling.

Notice the breakaway pressures are almost all negative. This is due to the fact that the areas on both side of the piston are different. For a 3 ¼" bore cylinder, the ratio between the piston area on the LDT side and the piston area on the rod

side is 1.2 and for the 2 ½" bore cylinder the ratio is 1.3. The forces are studied instead, because this ratio is included within the force. In addition, the force of gravity on the mass of the piston can also be easily introduced. For the 3 ¼" bore cylinder the gravity force is -5.9 lb_f, while for the 2 ½" bore cylinder the gravity force is -4.7 lb_f.

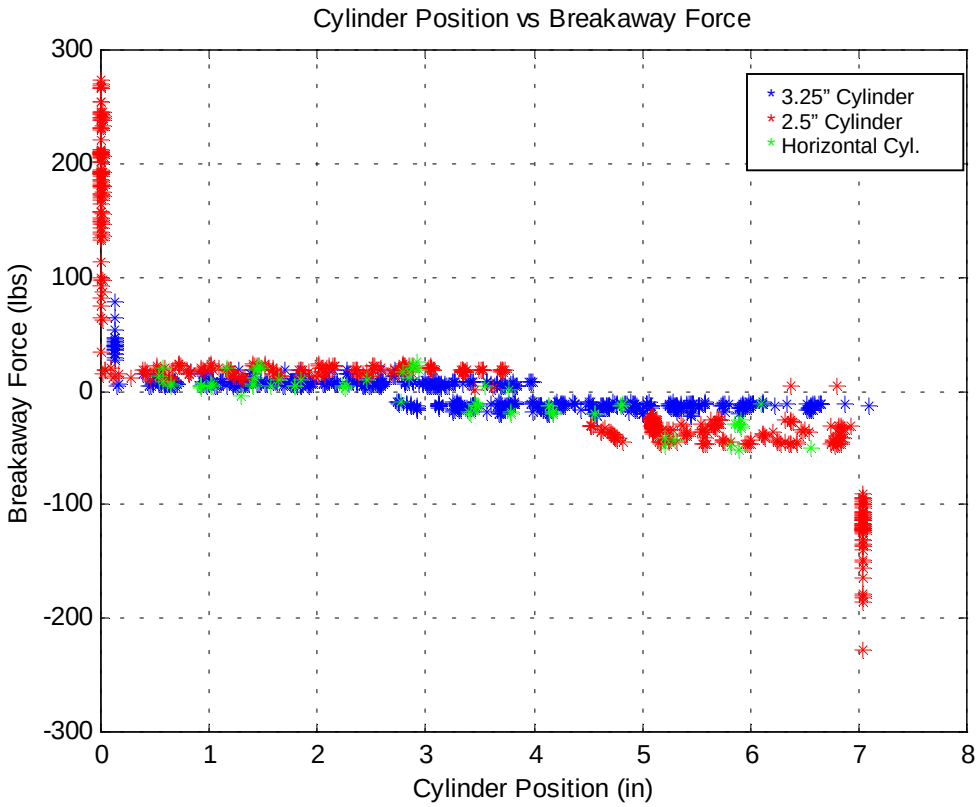

Figure 6-17: The breakaway force versus cylinder position, delineated by the cylinder bore size.

Figure 6-17 shows that the 2 1/5" bore cylinder has a higher breakaway force than the 3 ¼" bore cylinder. The horizontal cylinder breakaway forces confirm that the gravity force assumption is accurate, because they reside within the range of the vertical breakaway forces modified by the gravity force. Note that at the cylinder limits, the breakaway pressure becomes much higher. To better

view the breakaway forces away from the cylinder limits, the breakaway forces near the cylinder limits are omitted in Figure 6-18.

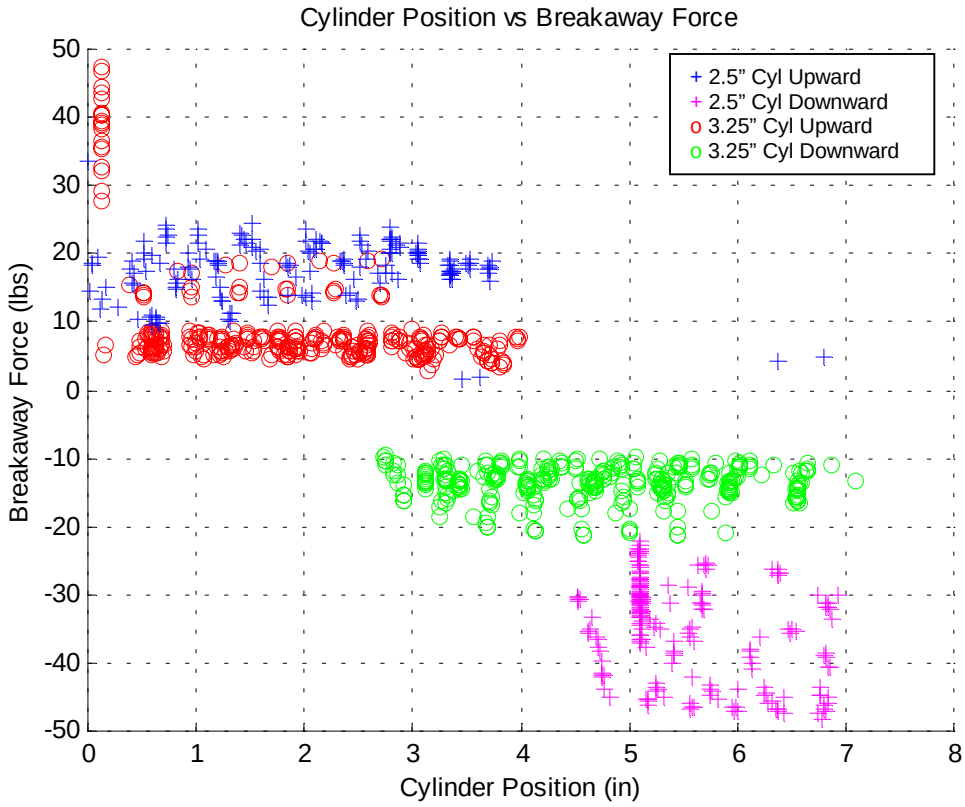

Figure 6-18: Breakaway forces versus the cylinder position for the areas away from the cylinder limits delineated by the cylinder size and direction of movement.

Figure 6-18 shows the 3 ¼" bore cylinder's breakaway force seems to stay near 8 pounds for extension and 12 pounds for retraction, while the 2 ½" bore cylinder's breakaway force averages at about 18 pounds for extension and 35 pounds for retraction. Remember that the friction breakaway is dependent on many environmental factors such as the amount of time the cylinders have run, the temperature of the oil, the thickness of the lubricant film on the rod, etc., so there will be some stray data points and large ranges for the sets of data.

When looking at the relationship between the operating pressure and breakaway force it was found that the operating pressure does not control the breakaway force, as shown in Figure 6-19.

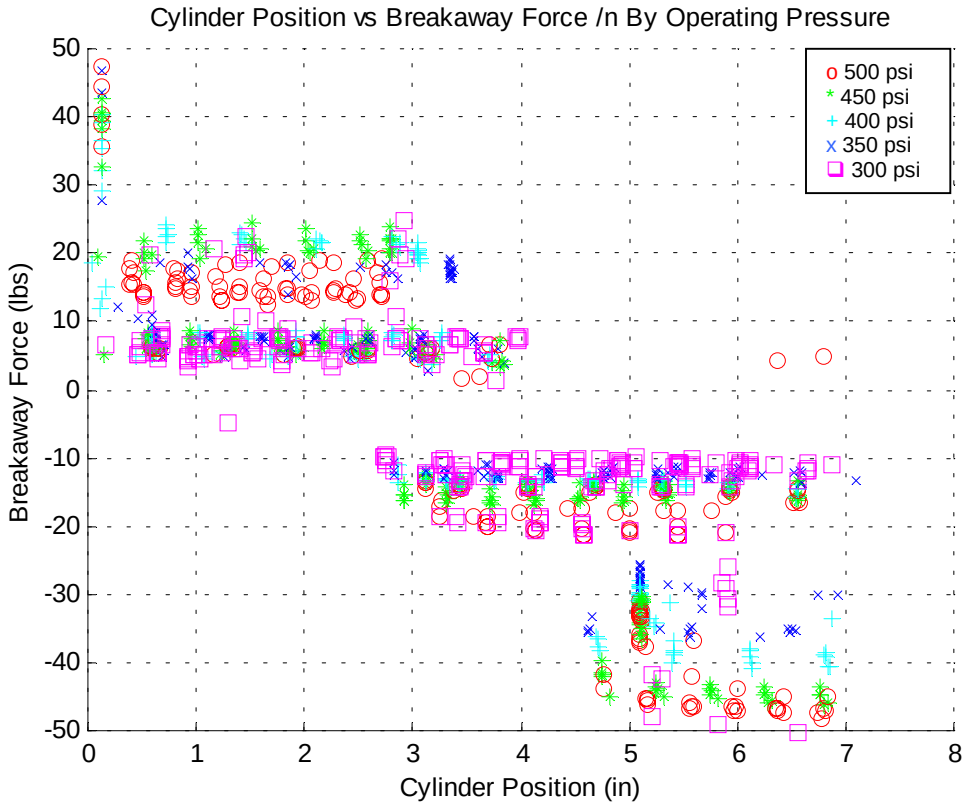

Figure 6-19: Breakaway force versus cylinder position delineated by the operating pressure the system is working at.

Figure 6-20: Force vs position and piston distance near a breakaway point.

Figure 6-20 depicts the piston position and the force across the piston near a breakaway. Note that the breakaway force nears 7 pounds and then the running friction is at about 5 ½ pounds. This confirms that there is little stick-slip in the hydraulic cylinder with the PTFE seals.

An interesting phenomenon occurred when these experiments were executed. When the input was a triangular wave, the cylinder would migrate upwards or towards full extension. This is expected due to the differing piston areas, but when the input was a square wave, the cylinder would migrate downwards or towards full retraction. This phenomenon was not expected it is most likely do to the varying flows to each chamber. The square wave inputs instructs the proportional valve to shuttle from the far left to the far right, while the triangular

wave instructs the proportional valve to move linearly from the left to the right. This could be an interesting phenomenon to study further.

6.6 Conclusions

Having an idea of the forces it takes to overcome static friction in a hydraulic cylinder is very important when designing high performance, motion control, hydraulic systems. The magnitude of the forces needs to be integrated into the controls of the system such that these breakaway forces are compensated for. These friction forces are difficult to understand using analytical means, so they are generally defined empirically. Empirical data of the breakaway pressures was found on the 2 ½" bore and 3 ¼" bore 3L Parker cylinders with low-friction seals. These seals were expected to not vary with operating pressure due to the configuration of the low-friction seals, and also have a breakaway force that is close to the running force across the piston.

It was found that the 3 ¼" bore Parker cylinder has a breakaway force range from 5 to 10 pounds in extension and has a breakaway force range from 10 to 20 pounds in retraction. The 2 ½" bore Parker cylinder has a breakaway force range of 10 to 25 pounds in extension and has a breakaway force range of 35 to 50 pounds for movement in retraction. The variation between the extension and retraction comes from the non-uniform rod seal, as well as the reduction of lubrication and introduction of foreign objects on the rod surface. The variation of breakaway forces between the 2 ½" and 3 ¼" bore cylinders is due to the differing circumference to cross sectional area ratios of the pistons. The 2 ½"

cylinder has a higher ratio therefore the forces will be higher. The varying seal designs may have an impact on the variation between cylinder sizes as well, with the 2 ½” cylinder most likely having smaller tolerances resulting in higher preloads requiring larger friction forces. At the cylinder limits, both the 3 ¼” bore cylinder and the 2 ½” bore cylinder saw breakaway pressures ranging from 150 to 210 pounds. This is due to the change in effective surface area when the piston is near the port opening.

Chapter 7: Future Research

The hydraulic test stand has been designed for future research that includes the mapping of the stability boundaries in design parameter space; developing advanced non-linear control strategies to expand the performance envelope; and studying the effects of various non-linear loads. To accomplish the future research, the hydraulic system will need a more powerful power unit than the power unit on the Parker Industrial Hydraulic Trainer. It will also need a new valve with a higher bandwidth, such as a servo-valve. In addition, the accumulators will need to be sized for the appropriate air content, and preload.

The breakaway friction forces and breakaway pressures can be incorporated into the non-linear analysis techniques. More in depth friction characterization may be needed. Testing with higher flow rates and varying velocity should reflect the Stribeck curve. To accomplish this testing a larger power unit and higher operating pressures are needed.

The interesting phenomenon of the cylinder creeping in extension with a triangular input and the cylinder creeping in retraction with a square input should be further researched. It should involve the varying flow pattern through the proportional valve used due to the variation of input. The square wave input moves the valve spool from one hard limit to the other quickly, while the triangular wave input moves the valve spool in a linear fashion.

References

Adams, Douglas R., and Randall Allemang. *20-MECH-781: Non-linear Vibrations Class Notes.* Department of Mechanical, Industrial and Nuclear Engineering, University of Cincinnati, Spring 2000.

Anderson, Wayne R. *Controlling Electrohydraulic Systems.* New York: Dekker, Inc., 1988.

Allemang, Randall. *Vibrations: Experimental Modal Analysis.* UC-SDRL-CN-20-263-662, Cincinnati, OH: University of Cincinnati, 1999.

Bay, John S. *Fundamentals of Linear State Space Systems.* Boston: McGraw Hill, 1999.

Beer, Ferdinand P., and Russell Johnston Jr. *Mechanics of Materials* 2nd Ed. New York: McGraw-Hill, 1992.

Blackburn, J. F., G. Reethof, and J. L. Shearer. *Fluid Power Control.* Massachusetts: The MIT Press, 1960.

Blau, Peter. *Friction Science and Technology*. New York: Marcel Dekker, Inc., 1996.

Blevins, Robert D. *Flow-Induced Vibration.* New York: Van Nostrand Reinhold, 1990.

Blevins, Robert D. *Formulas for Natural Frequency and Mode Shape*. New York: Van Nostrand Reinhold Company, 1979.

Brown, F. T. “Wave propagation in tubes with turbulent flows: Part I: Analytical models.” *Fluid Transmission Line Dynamics*. Ed. Franke, M. E. New York: ASME, 1981.

Brown, F. T. and R. E. Linney “Wave propagation in tubes with turbulent flows: Part II: Experimental Results.” *Fluid Transmission Line Dynamics*. Ed. Franke, M.E. New York: ASME, 1981.

Brusaw, Charles T., Gerald J Alred, and Walter E Oliu. *Handbook of Technical Writing* 5th ed. New York: St. Martin’s Press, 1997.

Elleman, Asko and Robert Piche. "A modified orifice flow formula for numerical simulation of fluid power systems." *Fluid Power Systems and Technology.* New York: ASME, 1996. Vol. 3: 59-63.

Fadel, Moustafa A. "Dynamic behavior of servo control systems under several operating conditions." Diss. Purdue University, 1999.

Federlein, Henry. "System Dynamics." *1981 Fluid Power Technical Update Seminar*. Aug 11-13, 1981. Ed. G. W. Krutz *et al*. West Lafayette, IN: Agricultural Engineering Department, Purdue University, 1981. 15-67.

Fitch, E. C., and I. T. Hong. *Hydraulic Component Design and Selection.* Stillwater, OK: BarDyne, 2000.

Fox, Robert W., and Alan T McDonald. *Introduction to Fluid Mechanics 4th ed.* New York: John Wiley & Sons, Inc., 1992.

Geankoplis, Christie J. *Transport Processes and Unit Operations 3rd ed.* Englewood Cliffs, NJ: Prentice Hall, 1993.

Heald, C. C. *Cameron Hydraulic Data: A Handy Reference on the Subject of Hydraulics and Steam.* 18th ed. Liberty Corner, NJ: Ingersoll-Dresser Pumps, 1998.

Healey, A. J. and D. A. Hullender. "State variable representation of modal approximations for fluid transmission line systems." *Fluid Transmission Line Dynamics.* Ed. M. E. Franke. New York: ASME, 1981: 57-71.

Henke, Russell W. PE. *Fluid Power Systems and Circuits.* Cleveland, OH: Hydraulics and Pneumatics Magazine, 1983.

Horve, Les. *Shaft Seals for Dynamic Applications.* New York: Marcel Dekker, Inc., 1996.

Iyengar, Dr. S. K. R. "Dynamic modeling of hydraulic systems." *1981 Fluid Power Technical Update Seminar*. Aug 11-13, 1981. Ed. G. W. Krutz *et al*. West Lafayette, IN: Agricultural Engineering Department, Purdue University, 1981. 68-127.

Johnson, Jack L. PE. *Design of Electrohydraulic Systems for Industrial Motion Control 2nd ed.* Cleveland, OH: Parker Hannifin, 1995.

Johnston, D. Nigel, and Derek K Longmore. "Rating of pump fluid-borne noise." *Fluid Power Systems and Technology.* New York: ASME, 1994. Vol. 1: 81-90.

Jordan, D. W., and P. Smith. *Non-linear Ordinary Differential Equations: an Introduction to Dynamical Systems. 3rd ed*. Oxford: Oxford University Press, 1999.

Kremer, Gregory G. "Improved methods for robust stability analysis of non-linear hydraulic control systems: a bifurcation based procedure." Diss. University of Cincinnati, 1998.

Krutz, Gary, John Schueller, and Paul Claar II. *Machine Design: For Mobile and Industrial Applications. 2nd ed.* Warrendale, PA: Society of Automotive Engineers, Inc., 1999.

Krutz, Gary. *ABE 435: Hydraulics Control Systems - Class Notes.* Agricultural and Biological Engineering Department, Purdue University, Fall 1997.

Longmore, Derek K., and D. Nigel Johnston. "Measurement of the dynamic properties of hose walls required for modeling fluid-borne noise." *Fluid Power Systems and Technology.* New York: ASME, 1997. Vol. 4: 105-111.

Margolis, Donald L., and Craig Hennings. "Stability of hydraulic motion control systems." *Fluid Power Systems and Technology.* New York: ASME, 1994. Vol. 1: 65-74.

Mayer, E. *Mechanical Seals 2nd ed.* New York: American Elsevier Publishing Co., Inc., 1973.

McCloy, D., and H. R. Martin. *The control of fluid power.* New York: John Wiley & Sons, 1973.

Merritt, Herbert E. *Hydraulic Control Systems.* New York: John Wiley & Sons, 1967.

Muller, Heinz K., and Bernard S. Nau. *Fluid Sealing Technology: Principles and Applications.* New York: Marcel Dekker, Inc., 1998.

Nasca, Robert A. *Testing Fluid Power Components*. New York: Industrial Press Inc., 1990.

Parker Hannifin Corporation. *Design Engineers Handbook-Bulletin 0224-B1.* Cleveland, OH: Parker Hannifin Corporation, 1979.

Parker Hannifin Corporation. *Hydraulic Component Sizing-Bulletin 0243-B1*. 11th printing, Cleveland, OH: Parker Hannifin Corporation, 1999.

Parker Hannifin Corporation. *Industrial Hydraulic Technology-Bulletin 0232-B1. 2nd ed*. 9th printing, Cleveland, OH: Parker Hannifin Corporation, 1997.

Parker Hannifin Corporation. *Industrial Hydraulic Valves – Catalog 2502/USA.* Cleveland, OH: Parker Hannifin Corporation, 1997.

Parker Hannifin Corporation. *Making the Choice – Selecting and Applying Piston, Bladder, and Diaphragm Accumulators – Brochure 1660-USA.* Cleveland, OH: Parker Hannifin Corporation, 1997.

Parker Hannifin Corporation. *Parker Actuator Products – Catalog 0106-4.* Cleveland, OH: Parker Hannifin Corporation, 1997.

Pease, Dudley A. *Basic Fluid Power*. Englewood Cliffs, NJ: Prentice Hall, Inc., 1967.

Quian, W., R. Burton, G. Schoenau, and P. Ukrainetz. "A comparison of a PID controller to a neural net controller in a hydraulic system with non-linear friction." *Fluid Power Systems and Technology.* New York: ASME, 1998. Vol. 5: 91-95.

Seireg, A. A. *Friction and Lubrication in Mechanical Design*. New York: Marcel Dekker, Inc., 1998.

Serway, Raymond A. *Physics: for Scientists and Engineers 3rd Ed*. Philadelphia, PA: Saunders College Publishing, 1992.

Shukla, Amit. "Stability analysis and design of servo-hydraulic systems under non-linear loads – a bifurcation study." Prop. for Diss. University of Cincinnati, 2001.

Stecki, Jacek S., and Andrzej Garbacik. *Hydraulic Control Systems: System Design and Analysis*. Melbourne: Fluid Power Net Publications, 2000.

Taylor, Sue E.M., and D. Nigel Johnston. "Experimental validation of pipeline models for laminar and turbulent transient flow." *Fluid Power Systems and Technology.* New York: ASME, 1997. Vol. 4: 99-104.

Thomson, William T., and Marie Dillon Dahleh. *Theory of Vibration with Applications. 5th ed*. Upper Saddle River, NJ: Prentice Hall, 1998.

Viersma, Taco. J., *Studies in Mechanical Engineering I: Analysis, Synthesis and Design of Hydraulic Servosystems and Pipelines*. Amsterdam, Netherlands: Elsevier Scientific Publishing Company, 1980.

Watton, John. *Fluid Power Systems: Modeling, simulation, analog and microcomputer control*. New York: Prentice Hall, 1988.

Zheng, Danian, Heather Havlicsek, and Andrew Alleyne. "Non-linear adaptive learning for electrohydraulic control systems." *Fluid Power Systems and Technology.* New York: ASME, 1998. Vol. 5: 83-90.

Other Hydraulic Systems References of interest:

Duleba, G.S., S.W. Ginsburg, and J.E Harrison. *Hydraulic System Modeling, Steady State Analysis, Simulation, and Control System Analysis Using a Lumped Mass Approach.* Seattle, Wash.: The Boeing Company.

Stringer, J. *Hydraulic Systems Analysis An Introduction*. New York: John Wiley & Sons, 1991.

Welty, James R., Charles E. Wicks, and Robert E. Wilson *Fundamentals of Momentum, Heat, and Mass Transfer. 3rd Ed.* New York: McGraw Hill, 1990.